AFRL-AFOSR-UK-TR-2013-0010

Microscopic optical characterization of free standing III-Nitride substrates, ZnO bulk crystals, and III-V structures for non-linear optics

Professor Juan Jimenez

Fundacion General de la Universidad de Valladolid
GdS OptronLab
Física de la Materia Condensada
Paseo de Belen 1
Valladolid, Spain 47011

EOARD Grant 10-3101

Report Date: March 2013

Final Report for 15 September 2010 to 14 September 2012

Air Force Research Laboratory
Air Force Office of Scientific Research
European Office of Aerospace Research and Development
Unit 4515 Box 14, APO AE 09421

REPORT DOCUMENTATION PAGE

Form Approved OMB No. 0704-0188

1. REPORT DATE *(DD-MM-YYYY)*	2. REPORT TYPE	3. DATES COVERED *(From – To)*
18 March 2013	Final Report	15 September 2010 – 14 September 2012

4. TITLE AND SUBTITLE

Microscopic optical characterization of free standing III-Nitride substrates, ZnO bulk crystals, and III-V structures for non-linear optics

5a. CONTRACT NUMBER

FA8655-10-1-3101

5b. GRANT NUMBER

Grant 10-3101

5c. PROGRAM ELEMENT NUMBER

61102F

6. AUTHOR(S)

Professor Juan Jimenez

5d. PROJECT NUMBER

5d. TASK NUMBER

5e. WORK UNIT NUMBER

7. PERFORMING ORGANIZATION NAME(S) AND ADDRESS(ES)

Fundacion General de la Universidad de Valladolid
GdS OptronLab
Física de la Materia Condensada
Paseo de Belen 1
Valladolid, Spain 47011

8. PERFORMING ORGANIZATION REPORT NUMBER

N/A

9. SPONSORING/MONITORING AGENCY NAME(S) AND ADDRESS(ES)

EOARD
Unit 4515 BOX 14
APO AE 09421

10. SPONSOR/MONITOR'S ACRONYM(S)

AFRL/AFOSR/IOE (EOARD)

11. SPONSOR/MONITOR'S REPORT NUMBER(S)

AFRL-AFOSR-UK-TR-2013-0010

12. DISTRIBUTION/AVAILABILITY STATEMENT

Approved for public release; distribution is unlimited.

13. SUPPLEMENTARY NOTES

14. ABSTRACT

GaN presents a large potential as an optoelectronic and microelectronic material. State of the art GaN devices are fabricated on epitaxial layers grown on foreign substrates, which results in a very large extended defect concentrations (typically >109 cm-2), which is detrimental to the performance and reliability of the devices, especially for high power operation. Advances in the material quality are necessary for the implementation of the next generation of light emitting diodes (LEDs), blue laser diodes (LDs), and high power electronics. The improvement of the GaN crystal quality can be achieved by the use of GaN substrates for homoepitaxial growth. A great deal of effort has been devoted to the growth of bulk GaN crystals. Among the methods used the ammonothermal growth (solvo-thermal process using supercritical ammonia as a solvent) appears as the most promising method for fabricating crystals with size and crystalline quality scalable to industrial processes. The advantage of this method consists of the low growth temperature (⍰550-600ºC), and the relative low pressure (⍰100-500 MPa). The disadvantage mainly concerns the high impurity concentrations related to the use of mineralizers. A complete optimization of these methods must consider different aspects, including a full characterization of defects, both including impurities and native defects, for which high resolution spatially resolved characterization techniques are necessary. Therefore, a study of the main defects involved in these materials is essential to the understanding of their main properties and to improve the growth methodologies, and the treatments necessary to optimize them. This grant shows repeated improvements in the subject materials by working with various strains, growth conditions, temperature variation, and impurities, and studies crystal growth parameters necessary to improve the crystalline quality of these crystals suitable for obtaining high quality substrates and to determine the interaction between Frenkel pairs and the crystal defects. Among the areas for documented improvements were: luminescence spectral characteristics, optimized excitonic emission vs deep level emission, CL data and the crystal growth parameters, defect incorporation in different growth sectors, surface properties, grain boundaries, influence of crystal defects on the Yellow luminescence and the incorporation of cations in different growth sectors of ammonothermal AlGaN crystals, thermal treatments in controlled atmospheres: influence of the treatments in the distribution of defects, grain boundaries in melt grown crystals, identification of defects. Ion implantation, and the Influence of thermal treatments on the properties of the domain walls. Selective etching using DSL (Diluted Sirtl applied with Light), and the stress distribution around the domain walls. This study shows how to improve the crystal quality of the OP GaAs crystals in order to minimize the optical losses, and for InGaSb bulk crystals.

15. SUBJECT TERMS

EOARD, Semiconductor materials, Nitride Semiconductors

16. SECURITY CLASSIFICATION OF:			17. LIMITATION OF ABSTRACT	18, NUMBER OF PAGES	19a. NAME OF RESPONSIBLE PERSON
a. REPORT	b. ABSTRACT	c. THIS PAGE			John Gonglewski
UNCLAS	UNCLAS	UNCLAS	SAR	32	19b. TELEPHONE NUMBER *(Include area code)* +44 (0)1895 616205

Grant FA8655-09-1-3073-1

Microscopic optical characterization of free standing III-Nitride substrates, ZnO bulk crystals, and III-V structures for non-linear optics

By

J.Jiménez,

Co-workers: V.Hortelano, O. Martínez, J.Anaya

GdS OptronLab

Física de la Materia Condensada

Edificio de i+d

Paseo de Belen 1

47011 Valladolid, Spain

jimenez@fmc.ua.es

Ammonothermal GaN crystals

GaN presents a large potential as an optoelectronic and microelectronic material. State of the art GaN devices are fabricated on epitaxial layers grown on foreign substrates, which results in a very large extended defect concentrations (typically $>10^9$ cm^{-2}), which is detrimental to the performance and reliability of the devices, especially for high power operation. Advances in the material quality are necessary for the implementation of the next generation of light emitting diodes (LEDs), blue laser diodes (LDs), and high power electronics. The improvement of the GaN crystal quality can be achieved by the use of GaN substrates for homoepitaxial growth. A great deal of effort has been devoted to the growth of bulk GaN crystals. Among the methods used the ammonothermal growth (solvothermal process using supercritical ammonia as a solvent) appears as the most promising method for fabricating crystals with size and crystalline quality scalable to industrial processes. The advantage of this method consists of the low growth temperature (~550-600ºC), and the relative low pressure (~100-500 MPa). The disadvantage mainly concerns the high impurity concentrations related to the use of minerailzers.
A great improvement of the internal quantum efficiency of GaN based devices can be potentially achieved by the suppression of crystal defects in homoepitaxial layers. The growth of GaN in supercritical ammonia has been demonstrated; however, the growth of large high quality GaN, free of defects, is challenging. State of the art ammonothermal GaN crystals present numerous macrodefects, e.g. parallel growth, twins, and crevices. Normally these defects propagate along the growth direction (c axis) and present different signatures for c^- face (N-terminated) and c^+ face (Ga terminated). Critical aspects are the seeds, which are crucial for the quality of the crystals; in particular, the crystals defects seem to be related to it. Also, the control of the impurities is a critical issue.

The presence of the defects determines the luminescence emission, which is quenched or drastically reduced by the extended defects; while the unequal incorporation of impurities and point defects introduce spectral signatures in the luminescence spectrum. In this context, cathodoluminescence (CL) is an unique tool for the characterization of GaN crystals, because it permits the visualization of the macro-defects, and permits to reveal the presence of impurities and point defects from their spectral signature, when the CL is used in the spectrally resolved mode.
The main challenges concerning the GaN susbtrates are:
Optimization of the growth rate
Improvement of the transparency
Control the incorporation of impurities

Macro and microdefects can be formed in the ammonothermal GaN crystals.
The macrodefects created depend on the growth sector:

N-face: *twins, inversion domains, hexagonal pits, crevices*

Ga-face: *columnar growth*

An important issue concerns the role of the seed in the formation of the defects.

Regarding the impurities and point defects, their incorporation is also conditioned by the growth facet. In principle, the N face presents a higher impurity concentration than the Ga face. The growth rate is about 3 times faster in the N-face than in the Ga-face. On the other hand there is a huge interest in the non polar facets.

One of the main objectives of the crystals is a drastic reduction of the crystal defects, as compared to the epitaxial layers in foreign substrates, e.g. sapphire. Fig. 1 presents the panchromatic CL images of an epitaxial layer grown on sapphire substrate, and an ammonothermal crystal. The crystal presents a homogeneous emission very different from the typical grain like CL distribution of the heteroepitaxy.

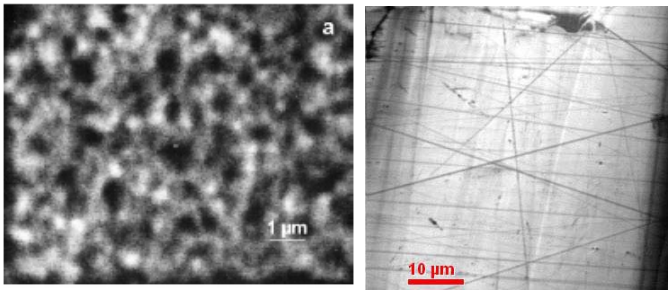

Fig.1. Panchromatic CL image of an epitaxial GaN layer grown on sapphire (left), panchromatic image of an ammonothermal GaN crystal (right).

Ammonothermal crystals

Ammonothermal GaN crystals were grown from alkaline solutions (2-6 M KNH_2 and $NaNH_2$) at temperatures in the 550-600 ºC range in high pressure autoclaves and supercritical ammonia. Thick hydride vapour phase epitaxy (HVPE) or ammonothermal seeds, cut from ammonothermal crystals were used as seeds. The wafers were cross-sectioned on (11-20) planes to investigate the properties of different growth sectors, Fig.2. The exposed plane (11-20) permits the study of the different growth sectors, in which different defect formation and impurity incorporation take place.

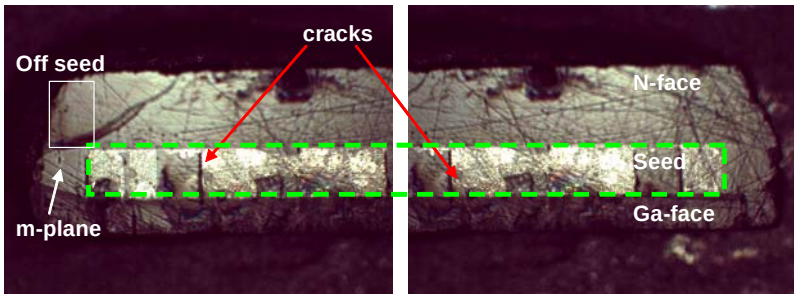

Fig.2. Stereoscopic image of the (11-20) plane of an ammonothermal GaN crystal.

The stereoscopic observation of the crystal reveals macrodefects such as columnar growth and cracks in the seed, Fig.1. The seed is the bright rectangle located in the center of the photo. Often, cracks are formed in the seed, which are likely due to stress accumulated in island coalescence (columnar growth), particularly on the c+ face. A non polar growth volume, grown on the *m*-plane (lateral) growth is also visible in the

stereoscopic image. One can also distinguish, (0001) and (000-1) volumes grown off-ssed

The study of the crystals was carried out by CL in both panchromatic and spectrally resolved modes, using a Gatan CL system (XiCLone) attached to a LEO 1530 field emission scanning electron microscopy (FESEM). The measurements were carried out at liquid nitrogen temperature, with 15 keV electrons. The detection is done with either a photomultiplier (PM) for panchromatic CL images acquisition, or a CCD detector for spectrally resolved CL measurements.

The panchromatic CL images permit to reveal the presence of large defects. The panchromatic images are contrast images, which are governed by the spatial distribution of the ratio between the radiative and non radiative recombination. In fact, it reveals contrast between defect-rich and defect-free areas. The internal quantum efficiency depends on the presence of crystal defects, and the concentration of impurities and point defects. Spectrally-resolved CL permits to observe emissions associated with specific point defects or dopants, allowing to study the distribution of those defects. In seeded, volumetric growth, the type of defects created will depend on the growth direction, growth temperature, and the presence of impurities in the solvent. Defects have also been associated with the quality of the seeds; it was claimed that they can be traced back to the seed. Normally they propagate along the c axis, and present different signatures for c^- face (N-terminated) and c^+ face (Ga terminated) [5,6].

Panchromatic CL images of the crystal of Fig. 2 are shown in Fig.3a. One observes the c+ and m–sectors free of extended defects, accounting for a good crystalline quality with low concentration of extended defects. However, large dark contrasted defects appear in the c- zone; note that they are not observed in the off-seed side, which suggests that the seed plays a relevant role in the formation of those extended defects, characterized by a high non-radiative recombination activity.

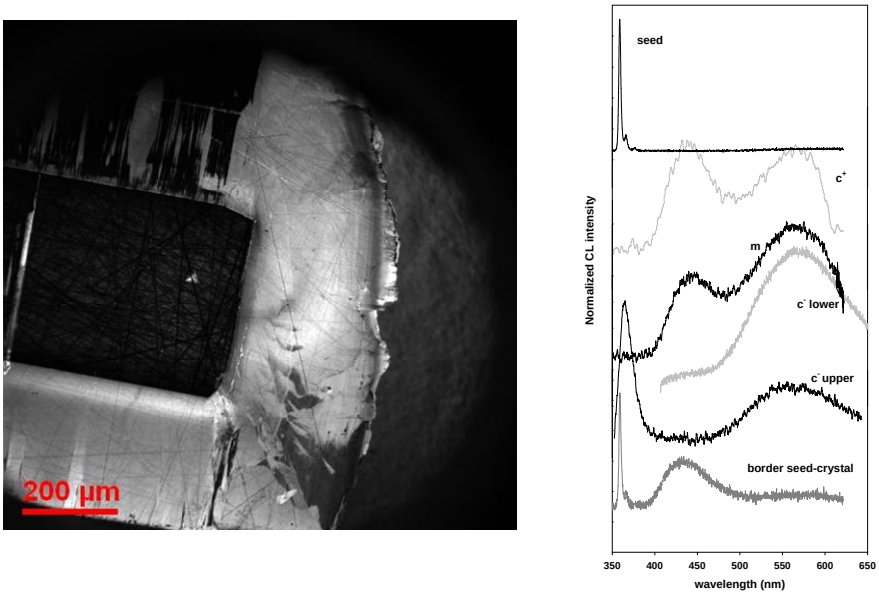

Fig.3. a) panchromatic CL image showing different growth sectors, b) CL spectra at different zones

Despite these extended defects, the high quality parts of the crystals did not show the typical grain-like dark/bright contrast observed in the CL images of the epitaxial layers, fig.1. This smooth emission points to good crystalline quality of parts of the ammonothermal crystals, those without extended defects, such as clusters of dislocations, or inversion domains. This is also confirmed by x-ray rocking curves, which for the best crystals give full widths at half maximum (FWHM) around 90-100 arcsec.

The spectra show evident differences between the seed and the ammonothermal crystal; which evidence the main flaw of the ammonothermal crystals at present. In spite of their excellent expectations, one of the problems concerning the ammonothermal crystals is the presence of impurities, and how are they incorporated to the different during growth. Local CL spectra are shown in Fig. 3b. The seed presents a well resolved near-band-edge (NBE) spectrum, with very low deep level related emission; however, the emission was not intense, probably because of the large concentration of dislocations. Peaks at 358.9 nm (FWHM= 2.7 nm), 366.3 nm (FWHM= 2.7 nm) and 376.6 nm (FWHM 2.3 nm) are observed, accounting for high crystal quality. The c^- sector is dominated by a broad yellow band (564.2 nm, FWHM=129.6 nm), with full absence of NBE. Far from the seed, the spectrum of the c^- sector shows NBE emission and the visible band; which suggests a reduction in the defect/impurity composition along the growth run, accounting for a significant reduction of the impurity concentrations and point defects in the top part of the crystal. Spectra in the c+ and m-plane sectors show the blue (BL) and the yellow (YL) band, without NBE emission. The spectrum at the border between the seed and the ammonothermal crystal shows the excitonic emission, but also a well marked BL, evidencing that the initial stages of ammonothermal growth incorporates the impurities giving the BL emission.

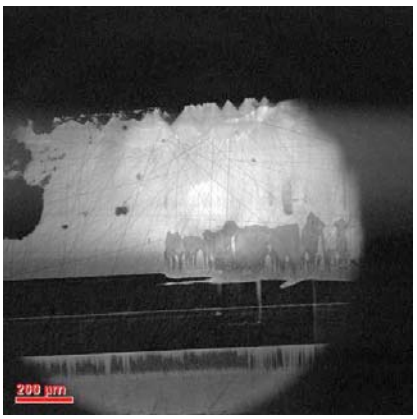

Fig.4. a) Panchromatic CL image of crystal B showing typical defects in c^- (top) and c^+ (bottom) crystal sectors.

The seed can be dissolved during the early stages of the ammonothermal growth; in Fig.4a one can observe in the panchromatic image of another sample (crystal B) the irregular interface between the seed and the ammonocrystal; the encircled zone in the c-side, Fig. 4a, shows something similar to an intrusion of the crystal inside the seed, which is probably the consequence of a partial dissolving of the seed in that zone. Coincidentally, the ammonocrystal grows vicinally on this zone presenting dark-contrasted defects that extend around 200 μm in height before restoring the uniform

growth observed on other parts of the seed. The c^+ side shows a tight array of parallel dark lines that extend 100μm (encircled zone in the c^+ side, Fig.4a), which can be associated with the typical columnar growth observed on the c^+ face.The CL spectrum exhibits changes along the growth axis which accounts for the improvement of the crystal quality, not only from the structural point of view, as revealed by the absence of macrodefects, but also by the changes in the incorporation of point defects along the growth run.

Close inspection of the CL spectra along the growth axis of the crystal was accomplished by taking spectra every 50 μm along the c- axis, from the top surface, down to the seed, Fig.5. One can see that the spectra in the region close to the seed are dominated by deep level luminescence emissions, BL and a contribution of YL, without NBE emission; the deep level (BL and YL) luminescence emission is very low in the seed, which suggests that the defects and impurities responsible for these emissions are generated solely by the ammonothermal growth. The NBE emission, including excitonic and shallow donor-shallow acceptor (SD-SA) transitions, starts to be observed at ≈200 μm away the seed; the BL emission is present all along the crystal, while the YL is enhanced with respect to the BL in the regions with extended defects. The emission intensity also increases along the growth axis, due to a decrease in the concentration of non radiative recombination centers.

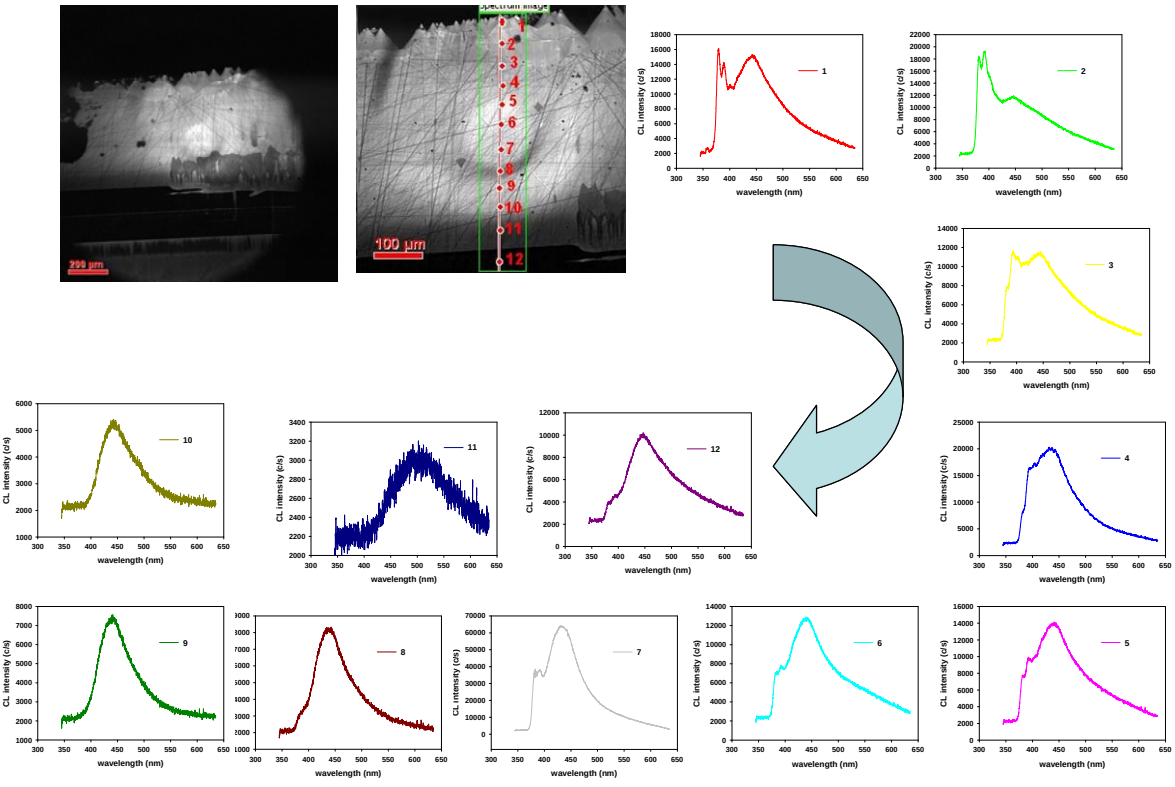

Fig.5. panchromatic CL images and spectra acquired every 50 μm across the c^- crystal axis

The CL spectra are indicative of the variation in the defect composition along the growth run. One can distinguish four spectral windows, Fig. 6.

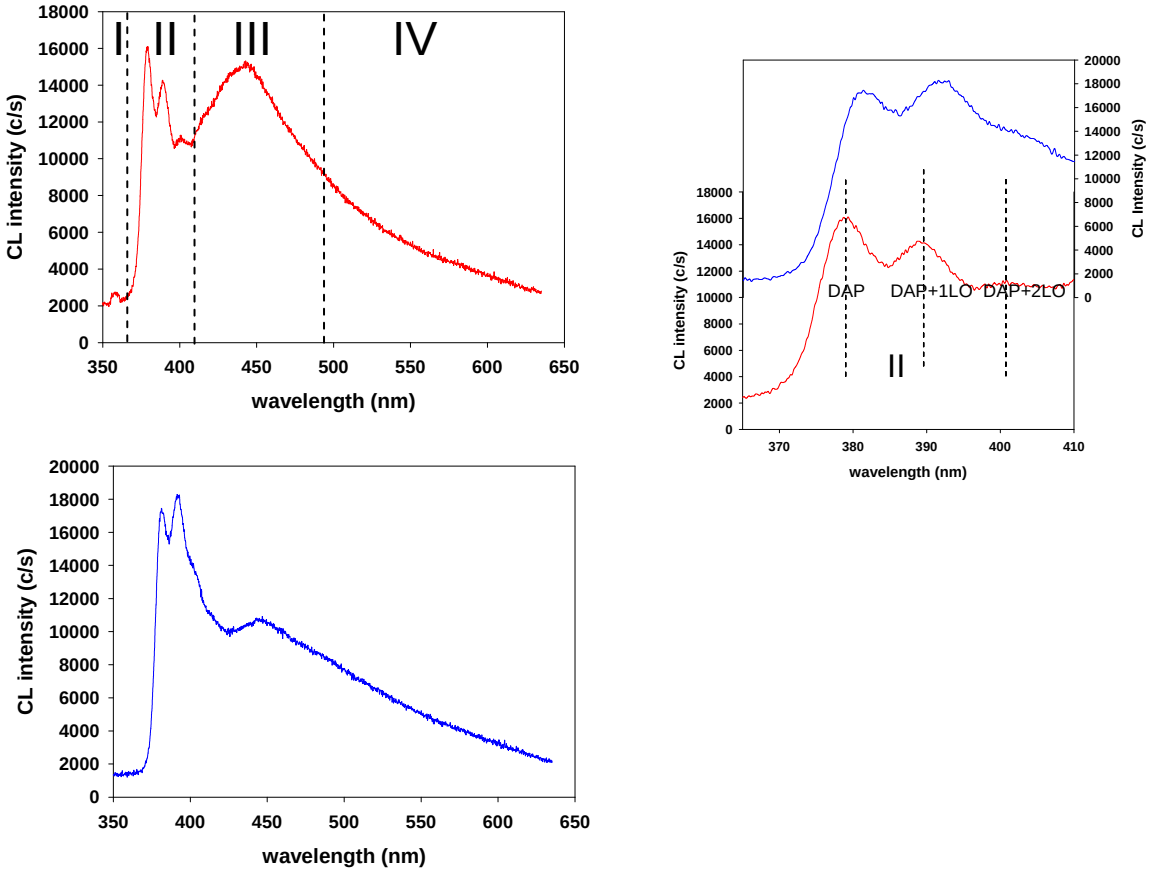

Fig.6. a) CL spectrum very close to the top surface of the N face crystal, b) CL spectrum at a deeper position, c) spectral window II of the two spectra.

The spectral zone I corresponds to the excitonic emission, which is scarcely observed in the (11-20) planes, probably because of poor polishing. In the zones close to the seed the spectra are dominated by deep level luminescence (DLE), spectral windows III and IV, mainly the blue luminescence peaking at 2.85 eV. The BL peak has been related to different impurities: Mg, C, Zn. SIMS measurements determined the presence of a non negligible concentration of Mg; therefore, one can relate the relative intensity of the BL band to the incorporation of Mg during the crystal growth. The quality of this crystal is poor, because macrodefects quench the emission of extensive parts of the crystal; the off-seed wings are not affected by a so large presence of macrodefects. The CL spectra do not exhibit excitonic emission, which reveals a high concentration of defects and impurities, which are responsible for the quenching of the NBE luminescence. It has been claimed that the absence of excitonic emission can be due to insufficient excitation in high resistive GaN (M.A. Reschikov, H.Morkoc; MRS Symp. Proc. 831, E3.7.1, 2005); however, it does not seem to be the case of this crystal, and the absence of NBE emission is rather probably due to a high concentration of defects and impurities.

It should be noted that the broad visible band presents significant spectral differences among the growth sectors. The GL and YL are usually associated with two charge states of the V_{Ga} -O_N complexes, giving donor acceptor pair transitions. Also, C has been claimed as the deep acceptor responsible for the YL in C-doped GaN (J.L.Lyons, A.Janotti, C.G.Van de Walle; Appl. Phys. Lett. 97, 152108 (2010)), C can incorporate in either Ga or N site, depending on the relative abundance of Ga and N, and the Fermi level position, when substituting N it was demonstrated to be a deep acceptor, which

can account for YL, even if it is not the alone cause of YL, which has been cxlaimed to be also related to the V_{Ga} -O_N pair.

The BL luminescence has been reported in Mg doped GaN, which cannot account for the BL of our samples. Also, it has been reported in Zn doped GaN, and was also observed in Si-doped n-type GaN. It was also associated with C (D.S. Green, U.K. Mishra, J.S. Speck; J. Appl. Phys. 95, 8456 (2004)). Green et al observed that the NBE emission was quenched when increasing the C concentration (D.S. Green, U.K. Mishra, J.S. Speck; J. Appl. Phys. 95, 8456 (2004)). Reschikov (M.A. Reschikov, H.Morkoc; MRS Symp. Proc. 831, E3.7.1, 2005) argued that the weak excitonic emission was due to low excitation intensity in very compensated samples; nevertheless, in our sample the shallow donor-shallow acceptor(SD-SA) transitions were also quenched, being dominated the spectrum by the BL and the GL-YL bands all over the sample including the seed. In fact, the NBE emission was observed in other samples under similar excitation conditions.

Region II corresponds to the 3.27 eV band and its phonon replicas, though the shape of the spectra measured in different regions of the crystal reveals the presence of several transitions, in addition to the 3.27 eV. The contribution of the different transitions depends on the position along the growth axis. Fig.6c shows the zone II of the spectrum for two different positions. The differences between both spectra evidence the presence of different DAP transitions. The blue plot shows two bands at 3.25 eV and 3.17 eV, slightly red shifted with respect to the ones of the red plot; also, in the blue plot the intensity of the 3.17 eV band is higher than the intensity of the 3.25 eV band, which points to a different DAP transition instead of the phonon replica. The origin of the SD-SA band at 3.27 eV is still controversial, although is usually related to the presence of oxygen; which is consistent with the high O contamination detected by SIMS. There is a low contribution of YL, which suggests some competition between the DAP luminescence and the YL. We will come back to this point later on.

The spectra in the Ga face side present different signatures as compared to the N-face. One observes that the spectra in the region with defects close to the seed mainly emit in the YL band (spectra #2, 3, 4); out of this zone the emission intensity increases and the spectrum is governed by the BL and a contribution of the YL (spectra # 5, 6, 7, 8, 9, 10) The DAP emission is only weakly observed in the top part of the sample (spectrum #10). The Ga-face incorporates more YL centers than the N-face. YL is often attributed to Ga-vacancy related complexes, and its presence can be considered as a witness of an effective nitrogen-rich stoichiometry, which means that the effective incorporation rate of N is higher in Ga-face than in the N face.

Fig.8 shows the panchromatic CL image close to the seed in the N-face side. One observes tha the extended dark defects, probably inversion domains do not arise from seed defects, but are generated during the first steps of the ammonothermal growth. Inside the red frame one observes that the the crystal presents a mosaic like structure, from which dark defects arise. In the blue frame one observes how the dark defects do not arise from the seed/crystal interface. It is highly probable that the seed was solved during the first stages of growth and that the recrystallization was responsible for the generation of the defects. The local spectra show that the dark defects present spectra similar to those observed in the Ga-face sector, Fig. 7; therefore, it is highly realistic to assume that the dark defects are inversion domains. The spectra close to the interface

are characterized by a YL-GL, which suggests that that region is rich in dislocations and other micodefects, which should account for the generation of the macrodefects, inversion domains. It should be noted that the inversion domains are only observed in the regions where the seed was solved. Therefore, the growth conditions avoiding seed solving are crucial for the obtaining high quality crystals.

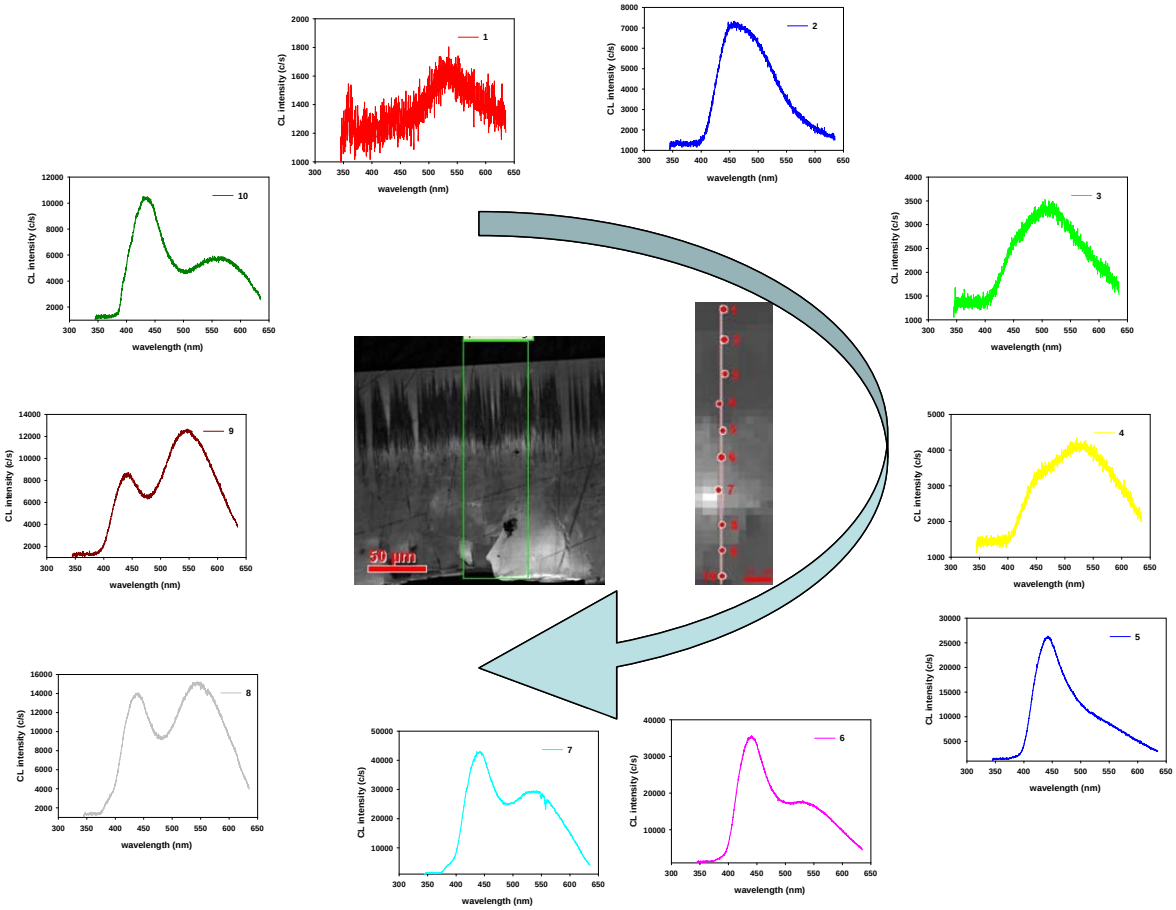

Fig.7. panchromatic CL image of the Ga face side, and local spectra taken at the points indicated in the red line.

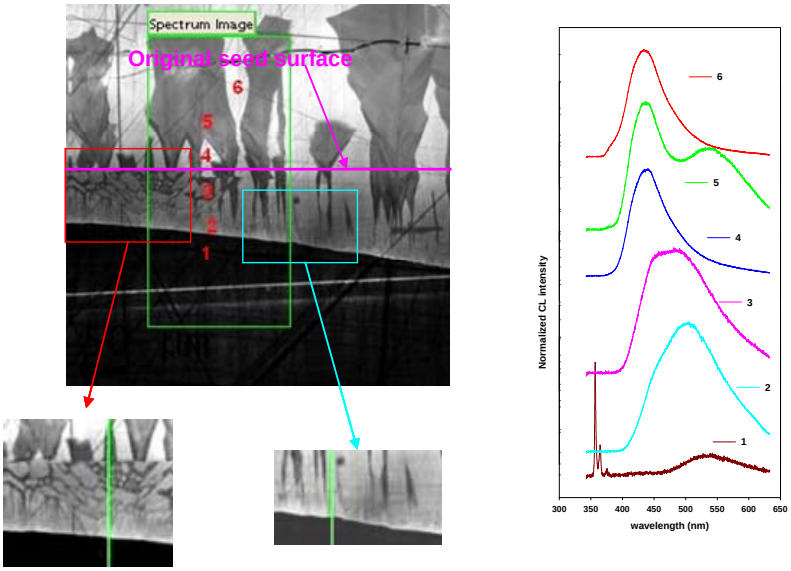

Fig.8. panchromatic images reveling the seed/crystal interface, and local CL spectra

The defects observed in the blue frame, Fig.8, do not arise from the interface, but they are generated inside the solved and recrystallized region. The pink line reproduces the original seed surface.

The etching of the top surface of the N-face zone reveals di-hexagonal pyramids, Fig.9.

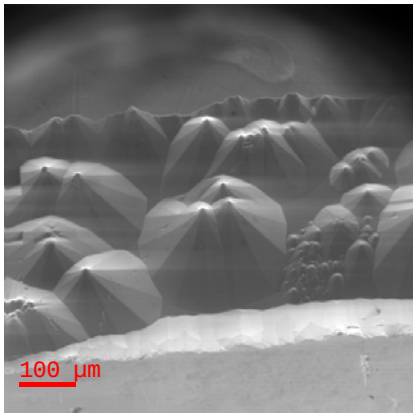

Fig.9. SEM image of the etched top surface

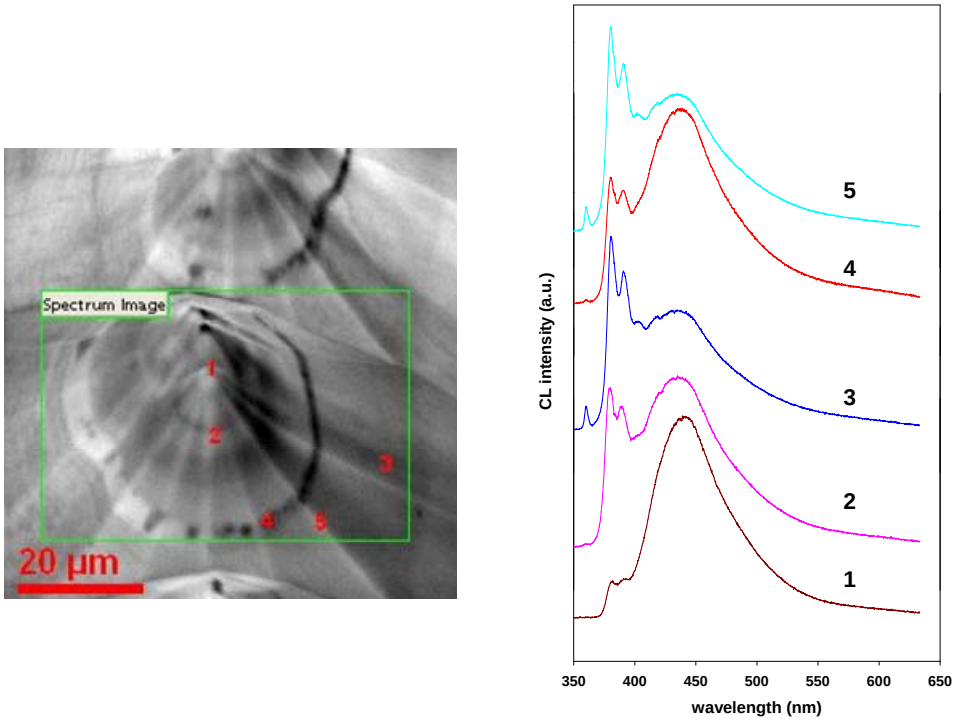

Fig 10. Panchromatic CL image of dihexagonal etch pits, and local spectra

The panchromatic CL image of the etch pits is shown in Fig.10. The CL reveals a dark pit surrounded by a series of contrasted rings, indicated by the red arrow, and smooth hillsides decorated with dark spots, fig.11.

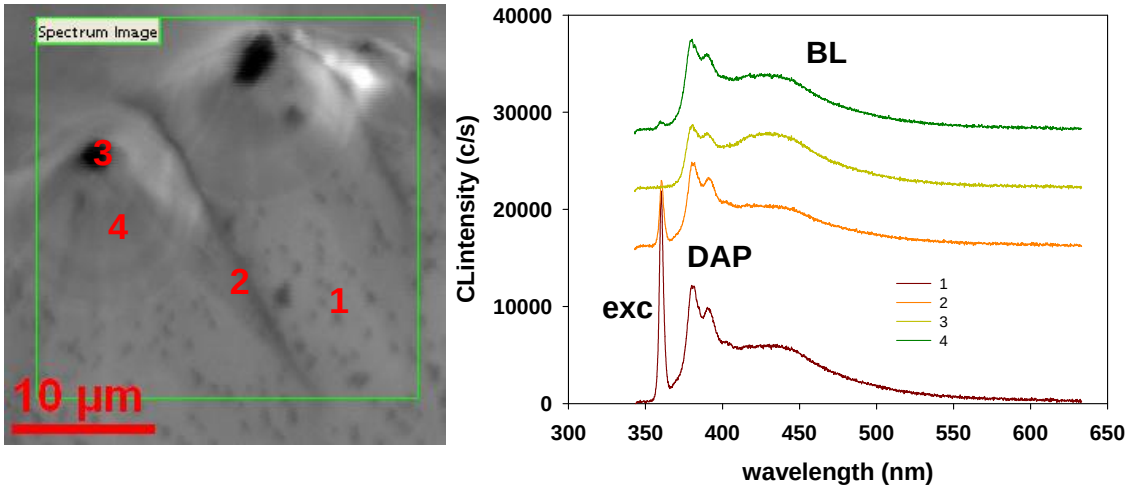

Fig.11. Etch pits and local spectra, where the spectrum image was carried out

Spectrum image analysis was carried out in order to study the incorporation of impurities and point defects around the dislocations. The images representing the total amplitude, the excitonic, DAP, and BL amplitudes normalized to the total amplitude are shown in Fig.12. One observes that the excitonic emission is quenched around the dark pit, the DAP is enhanced following the concentric rings, is quenched around the pit and enhanced again in the very pit, while the BL is fully anticorrelated with the DAP emission. The two defect related bands, DAP and BL are more intense around the pit, being their relative intensities reduced in the hillsides with respect to the excitonic emission.
The anticorrelation between the two defect bands suggests a competition for the formation of the two centers, which points to some elements common to the two defects.

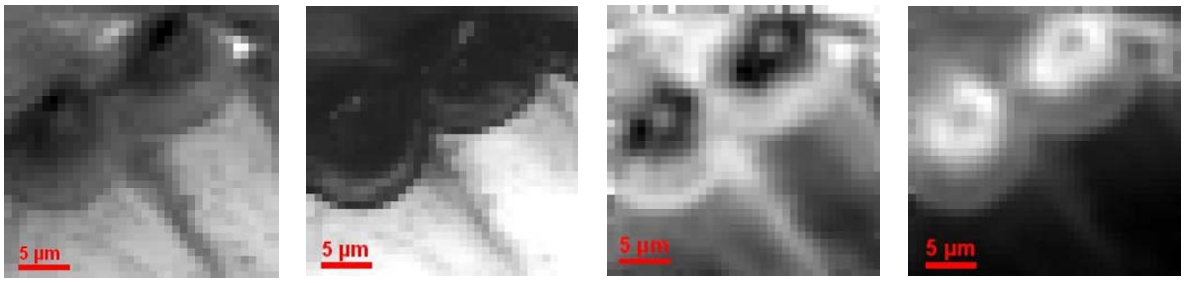

Fig.12. Total amplitude, and excitonic, DAP, and BL amplitudes normalized to the total amplitude

Sample L20. This sample permits to study the two sides, Ga and N, and the a and m growth planes. This sample presents an improved quality with respect to the other samples studied. Fig. 13 corresponds to the Ga face, the CL presents the typical columnar structure, corresponding to parallel growth. The spectra present a sharp excitonic emission and weak DAP and YL. On the other hand, the BL is very weak. The N face presents a smooth CL distribution, though some large inclusions are observed. They can be associated with the dark structures observed in sample 45, Fig.8 .

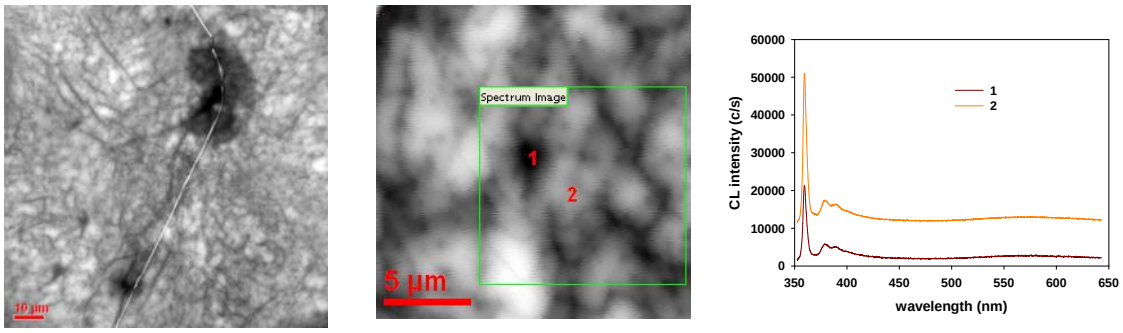

Fig.13. Pancchromatic images at two different magnifications of the ga face (top view), showing the typical columnar structure. Spectra at the points numbered in red in the pan CL image.

The spectrum imaging study of these structures is shown in Fig. 14.

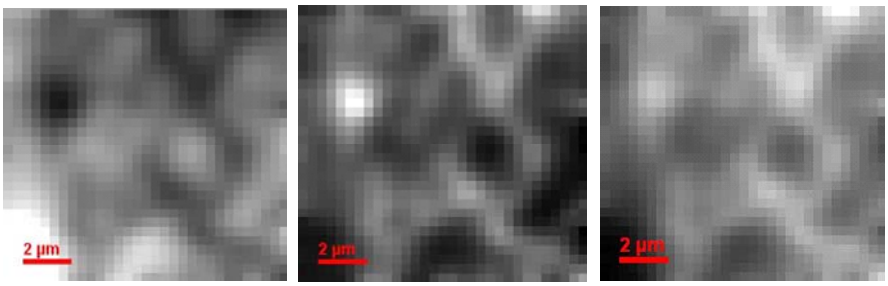

Fig.14. spectrum images showing anticorrelation between the excitonic emission and the defect related bands (DAP and YL). The defects are mainly decorating the boundaries of the columns.

The spectra recorded in the N face are different from those recorded in the Ga face, Fig. 15. The spectrum on the left corresponds to a macrodefect, see the insert of Fig.15, while the spectrum on the right corresponds to the regular N-face, with the spectrum very similar to the one observed in sample 45.

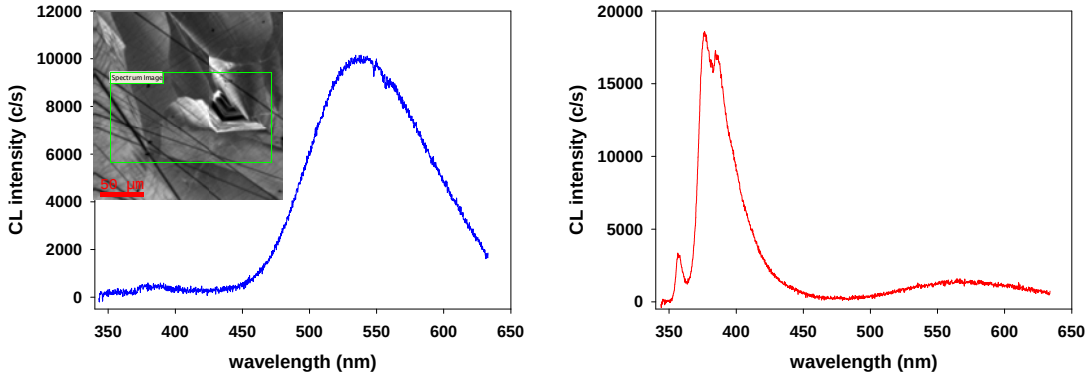

Fig.15. Spectra recorded in the N-face. Left) spectrum of a macrodefect, right) spectrum in regular N-face zones

One observes a high contribution of the DAP transition in the N-face with respect to the Ga face, while only YL is observed in the macrodefect.

Intrinsic defects in ZnO crystals

ZnO is very promising for UV optoelectronics, because of its bandgap (3.3eV at 300K), and large free exciton binding energy (60 meV). An additional advantage with respect to other wide bandgap semiconductors is the availability of ZnO substrates, necessary for the preparation of homo-epitaxial layers. The achievement of effective p-type doping constitutes today the main challenge for the practical use of ZnO. Stable p-type doping requires the control of the intrinsic defects, which can complex with impurities and also form compensating levels avoiding effective p-type doping [S.B.Zhang, S.H.Wei, A.Zunger; Phys. Rev.B 63, 075205 (2001). One of the main problems of ZnO refers to the poor knowledge about the electro-optical signature of intrinsic defects. Therefore, the generation of such defects and their subsequent characterization must provide valuable information about the role of the intrinsic defects. High energy e-irradiation (≈1MeV, at fluences ≈ 10^{17} cm^{-2}) is an effective method of creating point defects [L. S. Vlasenko and G. D. Watkins, Phys. Rev. B **7**1, 125210 (2005), F.Tuomisto, V.Ranki, K.Saarinen, D.C.Look; Phys. Rev. Lett. 91, 205502 (2003)]. Complementary to the e-irradiation, plastic deformation has been demonstrated to create intrinsic defects around the extended defects generated by indentation, or around scratch produced by either handling or polishing [V. Coleman, J. E. Bradby, C. Jagadish, and M. R. Phillips, Appl. Phys. Lett. **89**, 082102 (2006)., J. Mass, M. Avella, J. Jiménez, M. Callahan, D. Bliss, Buguo Wang, J. Mater. Res. **22**, 3526 (2007)]; this is also relevant in relation to the role played by dislocations. We describe herein the CL analysis of ZnO crystals, either, irradiated with high energy electrons, or plastically deformed by either Vickers indentation or lapping.

ZnO wafers cut from hydrothermal crystals were irradiated at room temperature with high energy electrons (1 MeV) at fluences of 10^{17} cm^{-2}. Vickers indentations with different loads ranging from 50 to 100 mN, were performed at room temperature on the (000$\underline{1}$) O-face of the ZnO samples. Also some scratches were selected for CL observation.

CL measurements at 80 K were carried out using a XiCLOne system from Gatan UK attached to a LEO 1530 field emission scanning electron microscope (FESEM), both panchromatic and spectrally resolved images were recorded. Hall effect measurements were carried out after e-irradiation.

A typical CL spectrum of as-grown ZnO crystal is shown in Fig.1. The spectrum can be separated in three spectral regions:

- ✓ the near band edge (NBE) emission with energies above 3.33 eV, including free and bound excitonic transitions
- ✓ the spectral range below 3.33 eV, usually associated with free to bound (e-A), donor acceptor pair (DAP) transitions, and/or phonon replicas
- ✓ the deep level emissions (DLE) in the green–red spectral range, which are associated with intrinsic defects

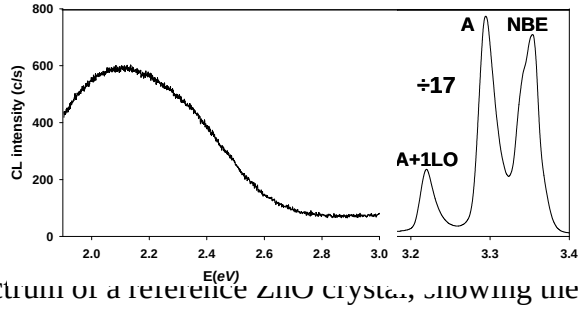

Figure 1 Typical CL spectrum of a reference ZnO crystal, showing the main luminescence emissions (T=80K, Eb=15kV).

The relative importance of the different bands depends on the sample growth method and post growth treatments. We will pay special attention to the band labelled A in the spectrum of Fig.1.

One observes several bands separated each other by ≈70 meV, which is the energy of the LO phonon (72 meV) in ZnO. Several phonon replicas at 3.23, 3.16 and 3.09 eV are resolved. The maximum of the A band is observed at around 3.30 eV; its origin is a matter of controversy, since it has been associated with:

- Donor-acceptor pair (DAP) transition (B.P.Zhang et al; Appl. Phys.Lett. 83, 1635 (2003))
- eA transition (E.Przezdziecka et al; Phys. Rev.B 76, 193303 (2007))
- First phonon replica of the free exciton transition, FX-1LO band (L.Wang, N.C.Giles; J. Appl. Phys. 94, 973 (2003))
- Structural defects (K.Thonke et al; Microelectron. J. 40, 210 (2009))
- Surface related excitons (J.Fallert et al; J.Appl. Phys. 101, 073506 (2007))

The shape of this band presents significant changes after both high energy electron irradiation, and in mechanical damaged.
Fig. 2 shows the CL spectra before and after e-irradiation. The main effect of the e-irradiation is a drastic decrease of the overall luminescence emission intensity, which is reduced by at least one order of magnitude, evidencing the generation of non radiative recombination centers. The second effect concerns the A band, which is split out in two bands peaking at 80K at 3.3154 (henceforth labelled P_D), and 3.3029 (labelled A) eV respectively. The two bands present phonon replicas, Fig.2. The P_D band is probably the band usually observed in the presence of structural defects (K.Thonke et al; Microelectron. J. 40, 210 (2009)).

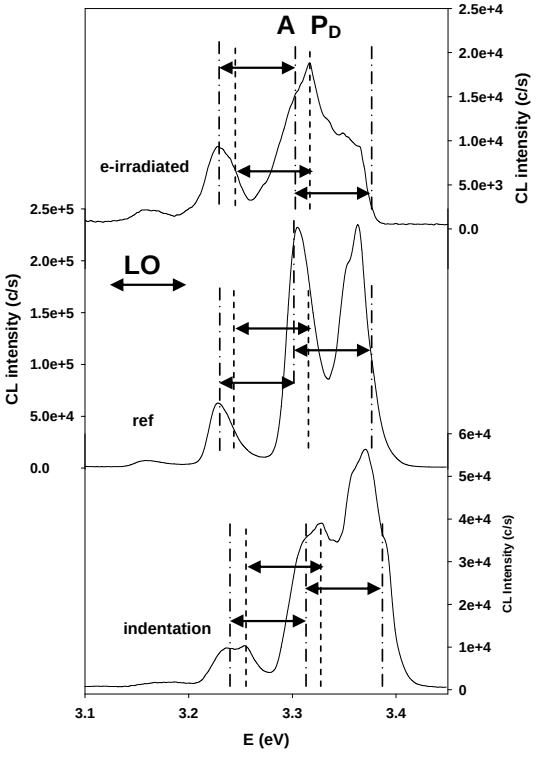

Figure 2 Spectra in the NBE and DAP spectral windows of e-irradiated, reference, and plastically deformed by Vickers indentation samples.

The CL spectrum in plastically deformed zones is also shown in Fig.2, the changes introduced in the spectrum are very similar to those observed in the e-irradiated samples. Therefore, one can argue that the same type of defects is being introduced in both cases

The P_D band and its phonon replicas are clearly distinguished from the A band. In the plastically deformed sample the free exciton (FA) is well observed, and it appears separated by the energy of the LO phonon with respect to the A band, which points to the A band as the 1LO replica of the free exciton in agreement with other reports (L.Wang, N.C.Giles; J. Appl. Phys. 94, 973 (2003), D.W.Hamby, D.A.Lucca, M.J.Klopfstein, G.Cantwell; J.Appl. Phys. 93, 3214 (2003)); however, the very high intensity of the A band does not support its phonon replica character.

One observes in the reference sample where the A band and its phonon replica are not separated by LO energy, but they are separated by a slightly larger energy, which is probably the consequence of the contribution of the P_D band in the high energy side of the A band in as-grown samples, which results in some uncertainty in the peak energy of the band. The P_D band seems to be present in as grown samples, both the e-irradiation and the plastic deformation reinforces its contribution, which suggests that the the P_D band is associated with an intrinsic defect.

The deep level luminescence is also changed after both treatments. One observes a decrease in the intensity of the deep level luminescence as a consequence of the generation of non radiative recombination centers; however, its relative intensity is enhanced with respect to the NBE emission, which supports a relative increase of the defects responsible for the deep level emission. On the other hand, one observes a shift to the orange red for both e-irradiated and indented, more marked for the e-irradiation, see Fig. 3. The orange red luminescence is associated with excess oxygen, in particular V_{Zn}, or O_i have been reported as the responsible for this band (H. C. Ong and G. T. Du, J. Cryst. Growth 265, 471 (2004)). The GL is related to oxygen defficiency, in particular V_O defects have been claimed as the centers responsible for the GL [K.Vanheusden, C.H.Seager, W.L: Warren, R.R.Tallant, J.A.Voigt; Appl. Phys.Lett. 68, 403 (1996)

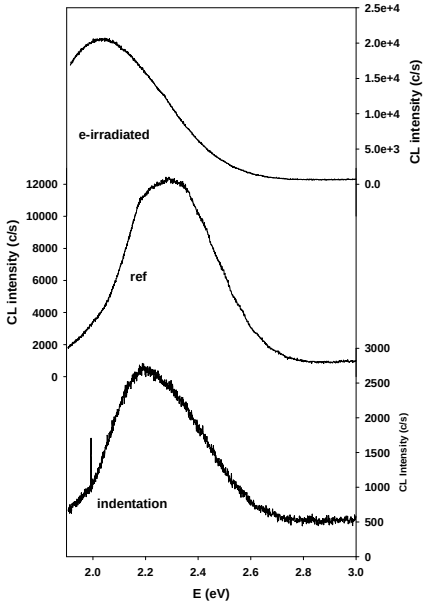

Figure 3. Spectra in the DLE spectral window of e-irradiated, reference, and plastically deformed by Vickers indentation samples.

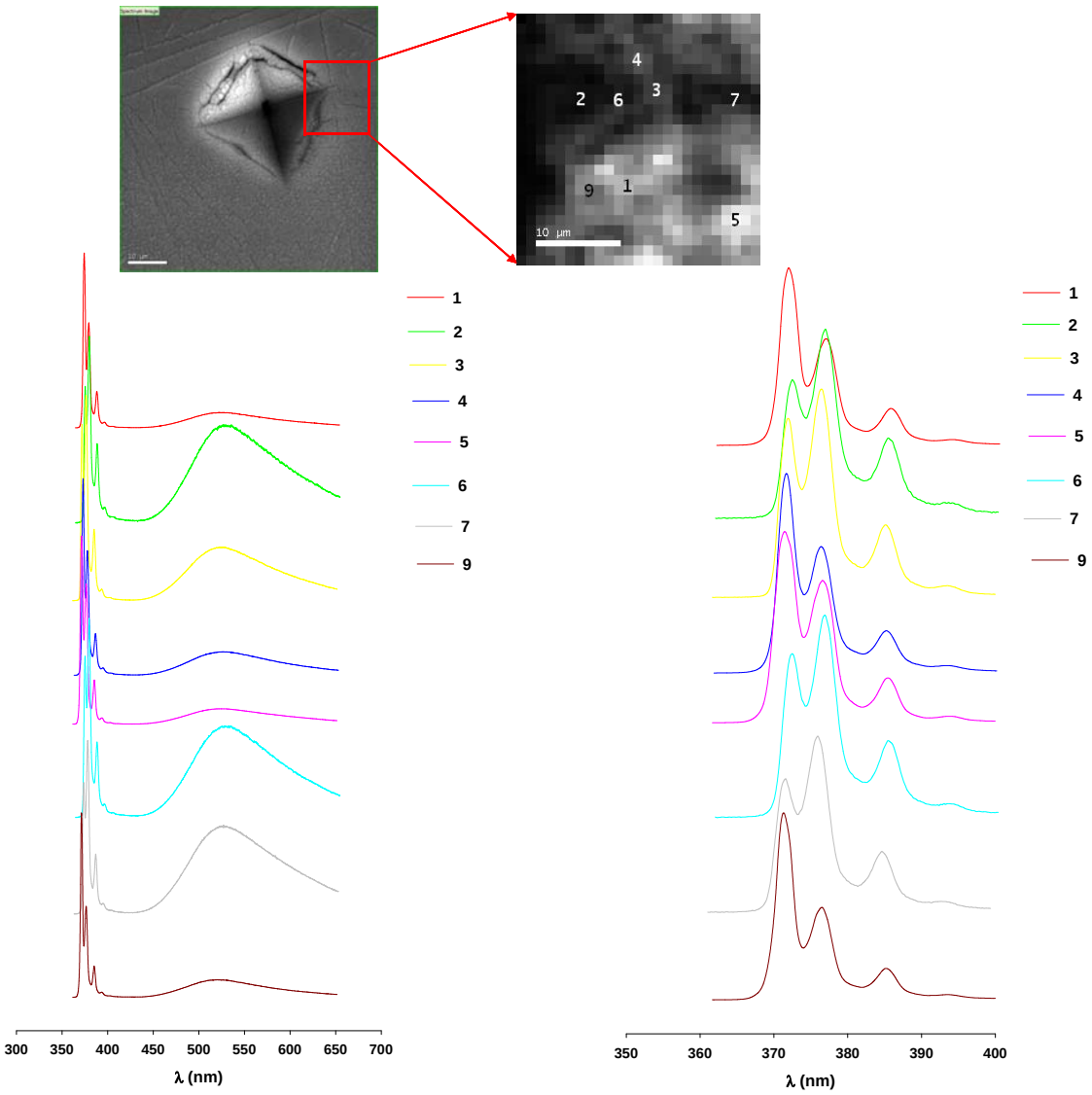

Fig.4. Vickers indentation, spectrum CL image, and local spectra at the points indicated in the image. The increase of the A+PD bands occurs in the same points where the DLE is enhanced.

The spectra acquired at selected points of an indented sample are shown in Fig.4, where one observes a clear correlation between the intensity of the A+PD band and the DLE intensity. This can be also observed in the spectrum images obtained on a zone shocked by handling, and equivalent to a low load indentation, Fig.5. One observes the spatial correlation between the PD emission and the DLE emission.
According to these results, both e-irradiation and plastic deformation generate non radiative recombination centers. Chichibu et al (S. F. Chichibu, T. Onuma, M. Kubota, A. Uedono, T. Sota, A. Tsukazaki, A. Ohtomo, and M. Kawasaki, J. Appl. Phys. 99, 093505 (2006))claimed that the NRRCs are related to V_{Zn} complexes, which is consistent with the generation of intrinsic defects by both procedures.. On the other hand, a relation between the V_{Zn}, and an band around 3.33 eV in ZnO films grown on sapphire substrates was established by Zubiaga et al (A.Zubiaga, J. A. García, F. Plazaola, F. Tuomisto, K. Saarinen, J. Zúñiga-Pérez, and V. Muñoz Sanjosé, J. Appl. Phys. 99, 05316 (2006). Positron annihilation studies have revealed that the main defects generated by e-irradiation are Zn vacancies (F.Tuomisto, V.Ranki, K.Saarinen, D.C.Look; Phys. Rev. Lett. 91, 205502 (2003)). The deep level luminescence also

supports the role of V_{Zn} defects as the main defects generated in both processes. It should be noted that the Hall effect measurements after e-irradiation revealed p-type, which can be ascribed to a relatively shallow acceptor related to V_{Zn} complexes.

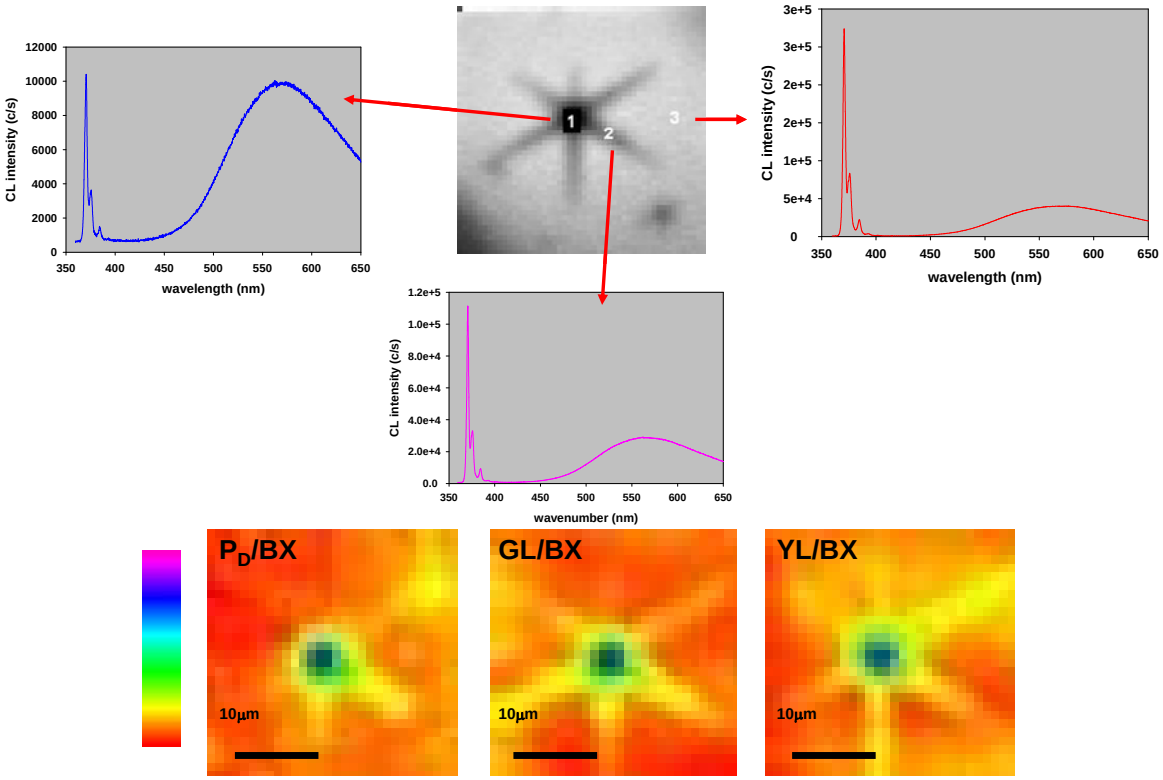

Fig. 5. panchromatic image of a mechanically induced defect, local CL spectra, and relative intensities of the PD and DLE bands evidencing their generation by mechanical damage.

e-irradiation and plastic deformation of ZnO crystals generate point defects with similar electro optic signature. Most of the changes induced can be tentatively related to the Zn sublattice defects.
In summary, V_{Zn} related defects seem to play a major role in the properties of electrical and optical properties of ZnO.

OP-GaAs crystals

Several samples have been studied:
Samples intentionally doped with Si (F9-28-10), both as –grown and annealed in arsine at 950ºC for 3 hours.
Samples specifically bevelled for exposing the wall plane in order to study the wall properties.
Samples grown at low temperature (F 4-18-11), sample p-type, $p=1.6*10^{16}cm^{-3}$. Sample 15 microns thick
Sample grown at high temperature (F 4-15-11), sample n-type, $n =3.9*10^{15}cm^{-3}$. Sample 16 microns thick, and sample F4-12-11, n-type, $n= 5.4*10^{15}cm^{-3}$, 51 μm thick.
The previous CL analysis of the OP-GaAs crystals was carried out with a Si-CCD detector, which the spectral range extends up to 1050 nm, but with very low response strength beyond 900 nm. One of the main clues for the optical propagation losses in OP-GaAs crystals concerns the presence deep levels. Therefore, the use of detectors with higher sensitivity beyond 900 nm is crucial to get information about deep levels; in particular, the lattice vacancies and their interaction with impurities should play a relevant role in the optical properties of the crystals. We present herein CL studies about the OP-GaAs crystals listed above, and recorded with an InGaAs detector array cooled with liquid nitrogen.

Samples intentionally doped with Si.

The CL spectra measured in different zones of the Si-doped OP-GaAs crystals are shown in Fig.1. These spectra were recorded in the domain wall. One observes the NBE emission peaking around 820 nm, a band peaking at 910 nm with a shoulder at 925 nm, these two bands are related to V_{Ga} related complexes. There is an additional band peaking around 950 nm, which exclusively appears in the domain wall, and preferably in the early stages of the HVPE growth, close to the seeds. The closest band reported in the literature is a band peaking at 1.31 eV, usually associated with Ga_{As} defects. In our case it peaks at 1.309 eV (946.5 nm). The NBE band is significantly broadened with respect to the undoped crystals, Fig.2, because of the band filling.

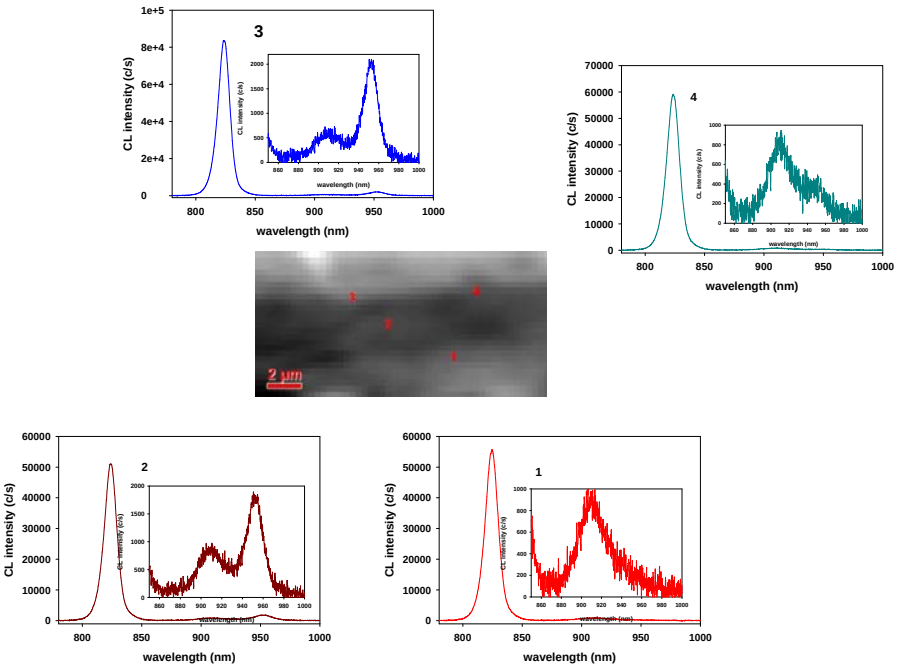

The luminescence of the walls is decreased with respect to the luminescence of the domains, but it is more efficient that the one expected from a pure antiphase boundary (APB), for which the expected quenching of the luminescence should result in a decrease of the luminescence intensity by several orders of magnitude (G. Brammertz et al.; J.Appl. Phys. 99, 093514 (2006)); however, in our domain walls we observe a quenching of less than 50 %, Fig.3; this anomalously low non radiative recombination activity of the antiphase boundaries suggests gettering of defects and/or impurities inhibiting the antibonds, As-As, and Ga-Ga, which are known to act as non radiative recombination centers.

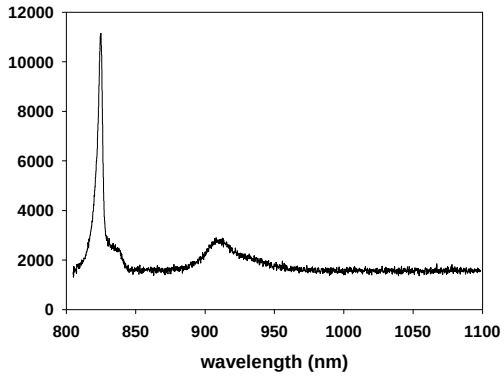

Fig.2. Typical luminescence spectrum of undoped GaAs

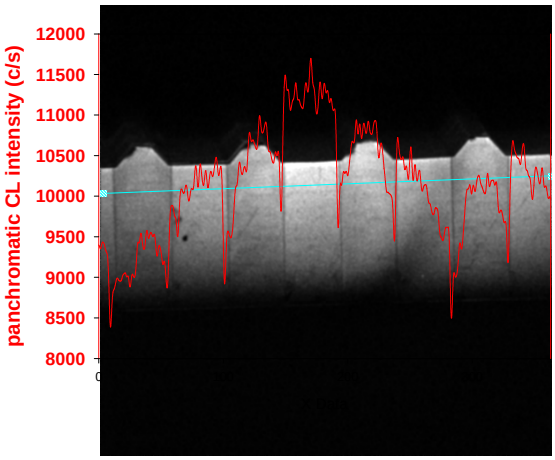

Fig.3. panchromatic CL image and intensity profile, showing the quenching of the luminescence at the domain walls. The overall shape more intense at the center than at the sides is an artefact due to the low magnification of the image.

Using the InGaAs array detector we improve our capability of detection in the low energy range of the spectrum. Typical spectra recorded in the domain walls (1) and the domain bodies (2) are shown in Fig. 4.

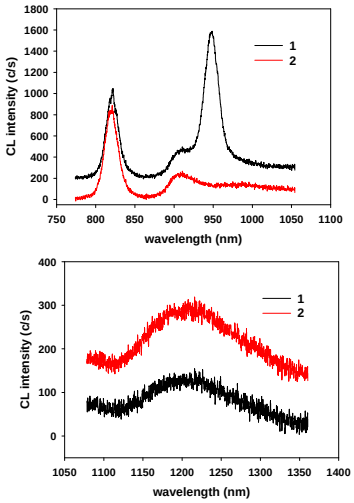

Fig.4. CL spectra recorded in the domain wall (1), and the domain body (2)

The spectra are recorded in two spectral ranges. One observes a weak band around 1000 nm (1.24 eV), which was not well appreciated with the Si-based CCD detector; this band is clearly observed in Fig. 5, when the detection is carried out with the InGaAs detector.

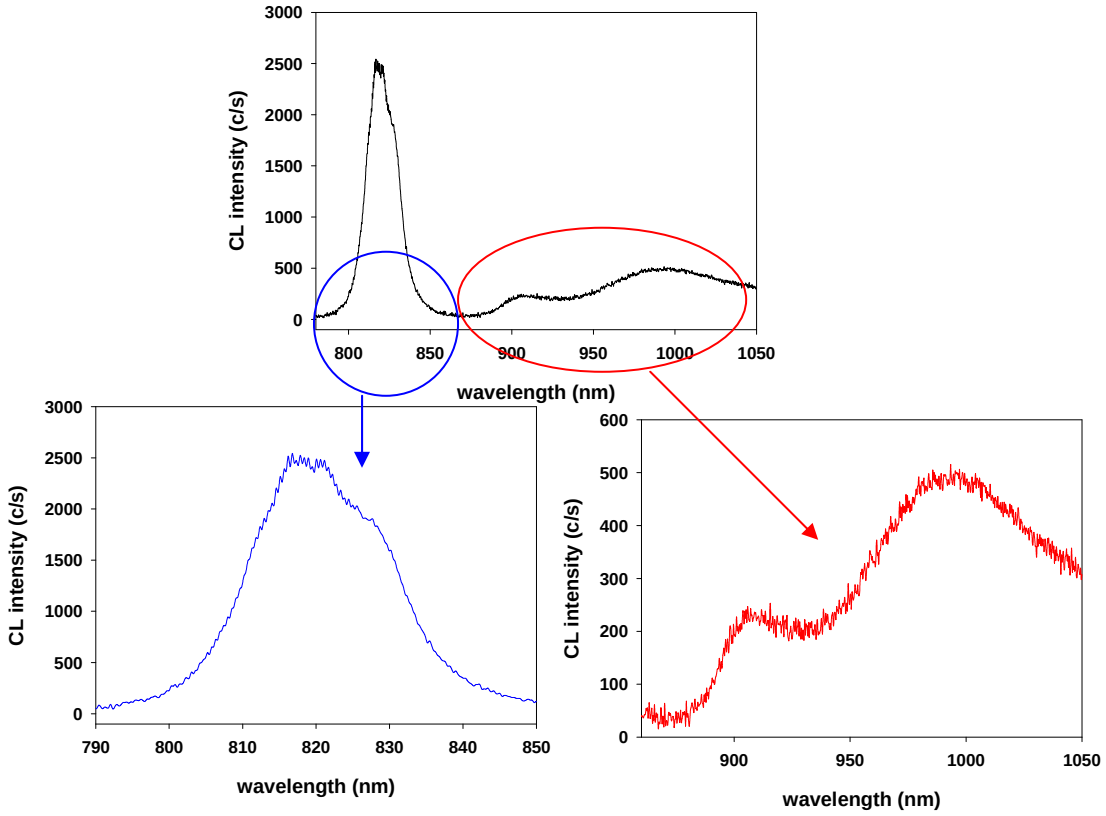

Fig.5. CL spectrum of Si-doped sample showing the details of the different spectral features

One observes that the NBE spectrum of the Si doped sample presents a higher complexity than the NBE spectrum of the undoped sample, Fig.2. One can observe the presence of the band corresponding to the Si_{As} acceptor related transition, peaking at 1.485 eV, see the shoulder in the low energy side of the NBE spectrum of fig. 5. On the other hand, the spectrum of the undoped sample does not exhibit the two deep levels related bands at 1100nm and 1200 nm, which are unambiguously related to Si doping.

The distribution of the two deep levels was studied, and the results are summarized in Fig. 6.One observes the typical behaviour of higher luminescence intensity in the [00-1] domain with respect to the [001] domain, though it is not so marked as for undoped OP-GaAs crystals; this is due to the higher incorporation of As in the [001] domains than in the [00-1] domains. The excess arsenic results in the formation of As_{Ga} related defects, though ion the case of Si-doped material it is in competition with the formation of Si_{Ga} donors. In bulk crystals these defects are usually labelled EL2; however, in the case of epitaxial layers the structure of the defect is not forcely the same; therefore, we will label them arsenic antisite related defects (AADR); which are formed by the absorption of As_2 molecules on Ga sites (J.C. Bourgoin et al.; Physica B 273-274, 725 (1999)). On the other hand, the peak wavelength and the FWHM of the NBE band show anticorrelation, higher λ_{peak}, and lower FWHM in [00-1] domain with respect to the

[001] domain. This can be interpreted in terms of the concentration of Si_{Ga} donors, which will be incorporated in a higher concentration in [001] domains, the concentration of free electrons would be higher in the [001] domains; which can be interpreted in two ways; there is a higher concentration of Si donors, Si_{Ga}, or the compensation ratio is higher, which can be explained by the lower formation of Si_{As} acceptor in the [001] domains as a consequence of the excess of As in this domain with respect to the [00-1] domain.

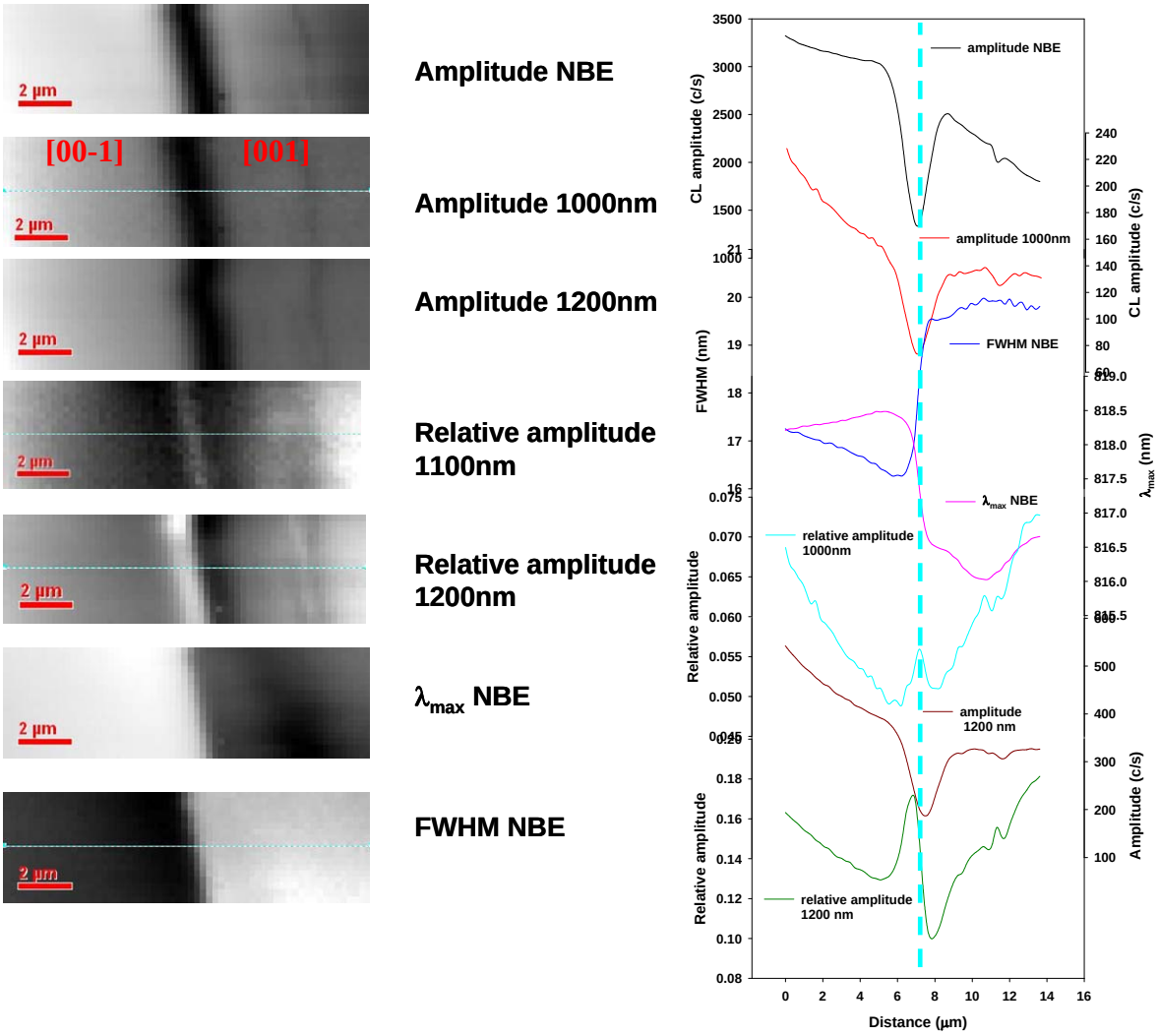

Fig.6. Spectrum images and transversal profiles in Si-doped OP-GaAs crystal

The two deep level related bands were also studied. The band peaking at 1000 nm, is usually associated with Si_{Ga}-V_{Ga} complexes (M.Holtz, et al.; Phys.Rev.B 50, 14706 (1994); L.Pavesi et al; Appl, Phys.Lett. 66, 2846 (1995)). The band peaking at 1200 nm is mainly related to Si_{Ga}-Si_{As} pairs (M.K.Hudait et al.; J.Appl. Phys. 83, 4454 (1998); E.P. Visser et al. J.Appl. Phys. 69, 3266 (1991)). It is interesting to observing the profiles of the two emissions, normalized to the NBE emission. If one looks at the Si_{Ga}-V_{Ga} complex related emission (1000 nm, ≅ 1.24 eV) it follows a similar distribution to the V_{Ga} related band peaking at 910 nm (1.36 eV) in undoped OP crystals, which confirms the presence of the V_{Ga} defects in te complex responsible for the 1.24 eV emission. The distribution of the 1.05 eV band around the domain wall is different, it is not symmetric at both sides of the wall, there is an increase of the Si_{As}-Si_{Ga} centers on

the region of the [00-1] domain nearby the wall, with respect to the same region in the [001] domain where the relative intensity of this band is decreased. This behaviour suggests that there is either a higher incorporation of Si in the [00-1] region, or that there is a lower concentration of As in this domain allowing the formation of Si_{As} defects and increasing the self compensation; which is consistent with the lower free electron concentration in the [00-1] domains, as deduced from the redshift of the NBE peak in the [00-1] domain with respect to the [001] domain. Indeed, the higher incorporation of Si is not consistent with the distributions observed for the λ_{peak} and the FWHM of the NBE band, which point to the opposite behaviour; therefore, the higher incorporation of Si_{As} could be related to the lower incorporation of As in the [00-1] domain, as already reported for undoped OP GaAs crystals.

The band at 950nm usually observed at the domain wall in undoped OP-GaAs crystals is also observed in the Si-doped sample; Fig. 7 shows the image of the domain wall (the plane of observation corresponds to the domain wall in this image) for the three emissions, NBE, 910 nm and 950 nm bands respectively, were the relative intensities of the three bands with respect to the total emission are mapped. The profiles across the horizontal line are shown in Fig. 7.

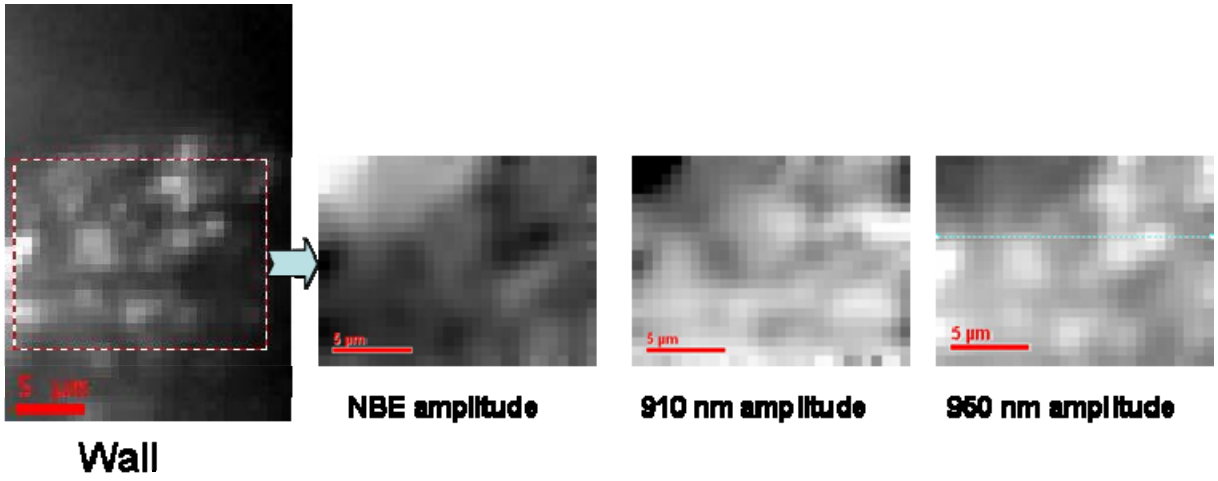

Fig.7

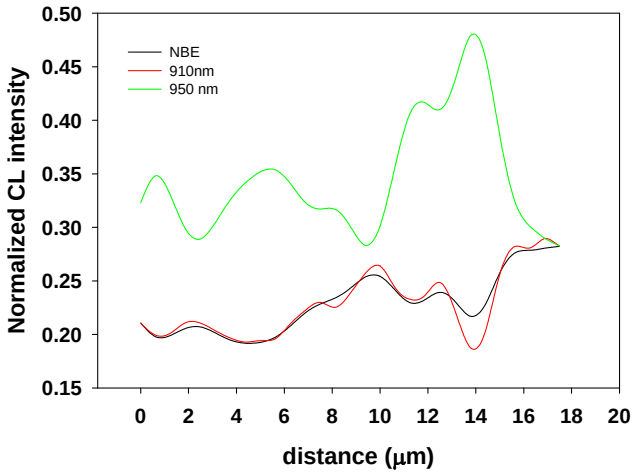

Fig.8. panchromatic and spectrum images of the domain wall of Si-doped OP-GaA, the lower plot corresponds to the profiles across the line indicated in the right image.

The emission at 950 nm is well observed with the InGAs detector, its distribution shows an island like structure, Fig. 7. The emission of the 950 nm band is anticorrelated with the two other bands, see the profiles in Fig.8, evidencing the recombination competition between the defects responsible for the 950 nm band and the other bands. The 950 nm band is mainly observed in region close to the seeds and then progressively disappears, which suggests that the stoichiometry could play a relevant role in the defects giving the 950 nm band. In fact an evolution of the CL contrast is observed along the growth axis in the OP-GaAs crystals, which can be explained by the change in the effective [Ga]/ [As] ratio because of the parasitic nucleation.
An equivalent crystal was annealed at 950ºC in arsine for 3 hours. There are significant spectral changes, Fig.9, shows two CL images corresponding to equivalent parts of the samples, as-grown and annealed) and the corresponding CL spectra.

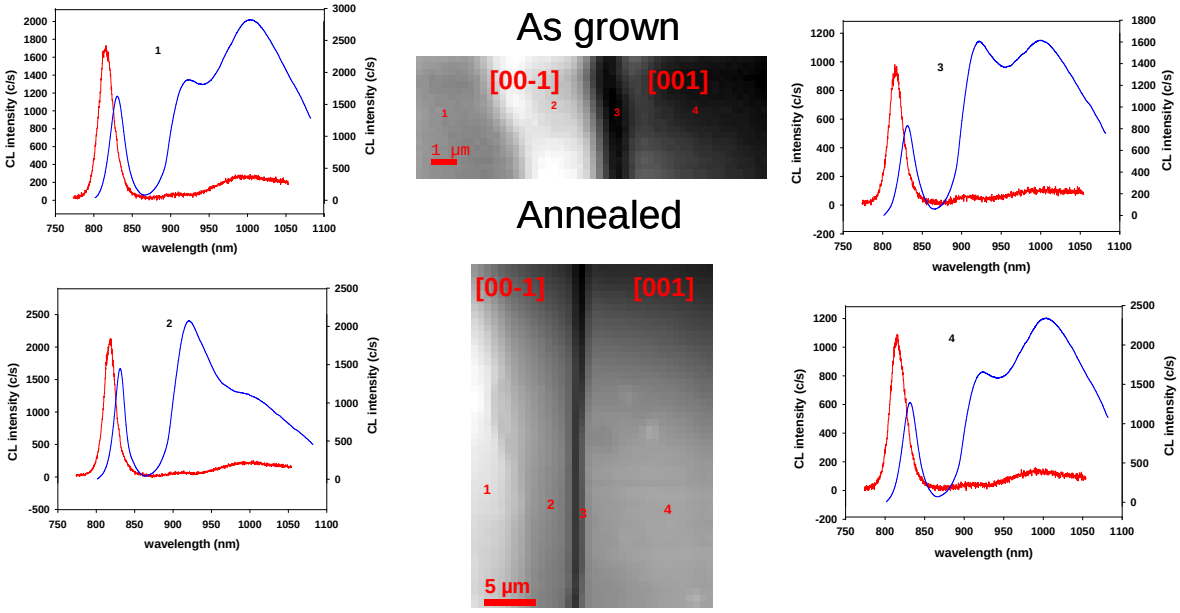

Fig.9.Panchromatic images of the as-grown and annealed Si-doped GaAs samples, and local spectra.

The evolution of the spectrum is consistent with the results reported in the literature for the annealing of Si-doped GaAs in As overpressure (N.H. Ky et al; J.Appl. Phys. 70, 3887 (1991)). The Si_{Ga} donors form complexes with V_{Ga}, which accounts for the electric compensation
The CL spectrum of the annealed samples presents the NBE band shifted to the red in relation to the as-grown sample. A braod and intense band peaking around 925 nm (1.34 eV), which has been associate with V_{Ga}, and a strong band at 1030 nm (1.2 eV), which is the Si_{Ga}-V_{Ga} related band. The result of the annealing in arsine is an increase of the V_{Ga} concentration, which accounts for the strong bands above mentioned. Furthermore the NBE is reduced and red shifted with respect to the as-grown sample, but also with respect to the undoped samples, Fig.2; which suggests that the NBE is dominated by e-A transitions, where the acceptor level might be Si_{As}. The spectral parameters of the annealed samples are represented in Fig.10. One observes differences with respect to the as-grown samples, Fig.6. The FWHM of the NBE band presents a similar distribution as for the as-grown sample. The peak wavelength however does not show the same trend, and presents smaller variation, being the main shift observed at the domain wall. The NBE is enhanced at the wing formed by the (00-1) domain, which does not support the

relation of the NBE band with the Si_{As} acceptor level. The two bands related to Si_{Ga} complexes, Si_{Ga}-V_{Ga}, and Si_{As}-Si_{Ga}, peaking at 1000 nm and 1200 nm are reduced at the (00-1) wing, because of the depletion of Si_{Ga}, in that region. However, the band associated with $V_{Ga,}$ defects (925 nm) is enhanced in the wing, because of the increase of V_{Ga} defects under As rich annealing, and the low complexing with Si because of the lower concentration of Si in that region, see the data of the as-grown sample in Fig. 6.

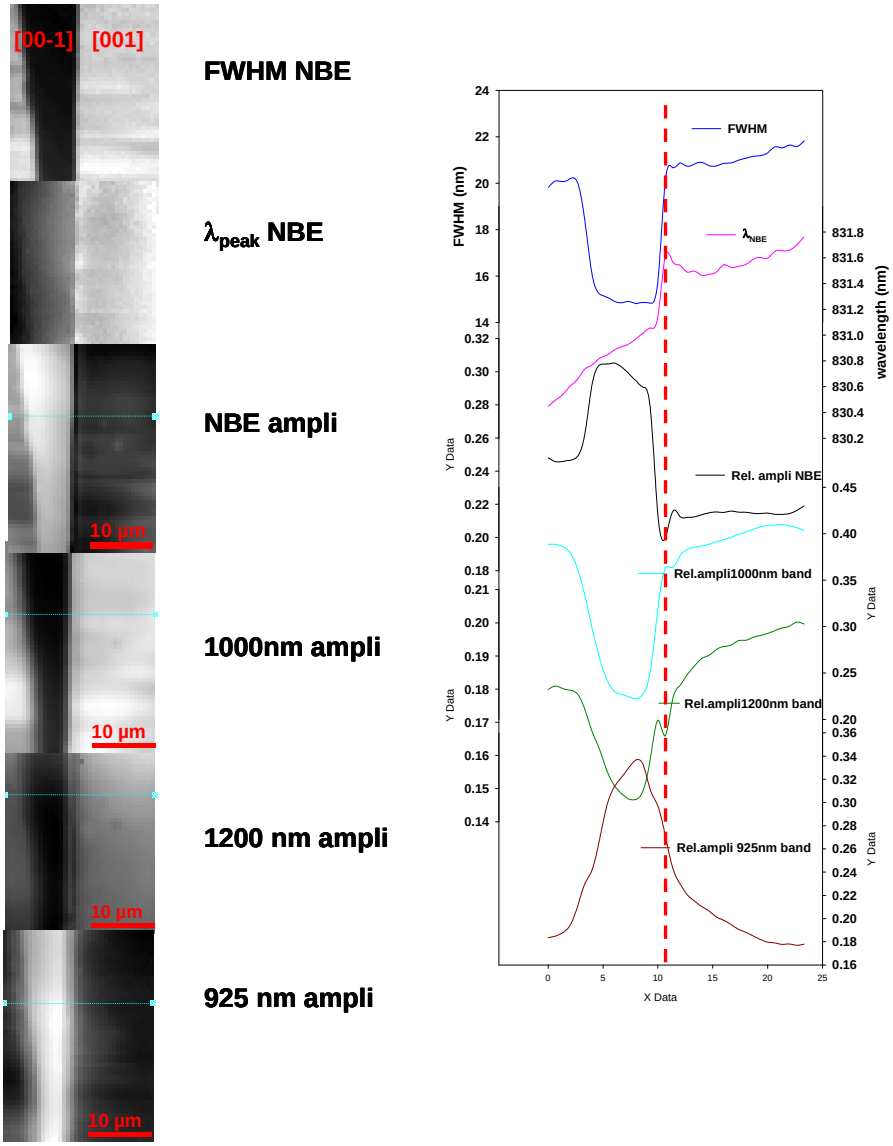

Fig.10. Spectrum images of the main CL parameters in annealed Si-doped OPGaAs sample, and transversal profiles

A comparison between the as-grown and annealed samples is shown in Fig.11. Note that the band labelled B, is not the same for both samples. The decoration of the domain walls with defects appear clearly illustrated in the distribution of the different bands; in particular, the domain wall is highlighted after annealing. Note that they are normalized to the total emission. While the as-grown sample presents dominant NBE emission, the annealed sample presents a high contribution of the V_{Ga} related bands, because of the

generation of V_{Ga} defects. It should be noted that the contrast of the wing with respect to the in the [00-1] domain is enhanced by the annealing.

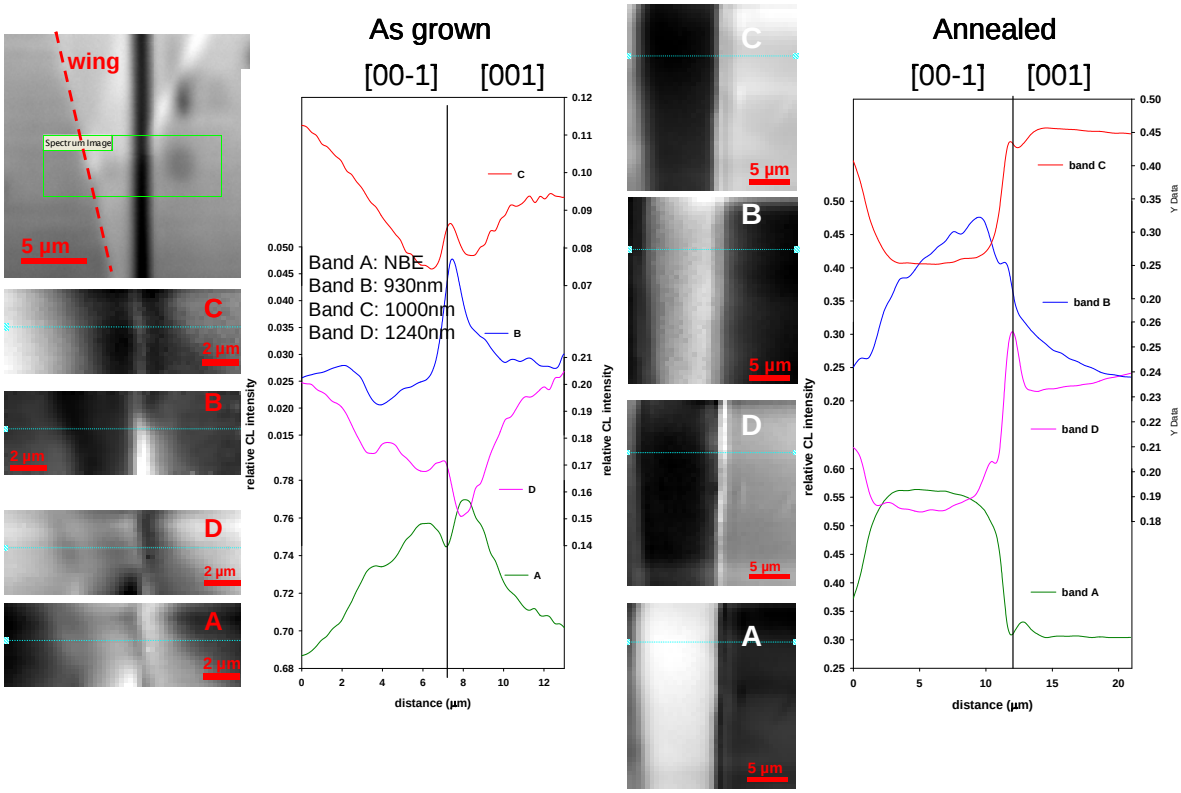

Fig.11. Comparative of the relative intensities of the main bands in as-grown and annealed Si-doped samples, the profiles show the transverse distribution of the bands.

Influence of growth temperature

Samples grown at low temperature (F 4-18-11), sample p-type, $p=1.6*10^{16}cm^{-3}$. Sample 15 microns thick.
Sample grown at high temperature (F 4-15-11), sample n-type, $n=3.9*10^{15}cm^{-3}$. Sample 16 microns thick.

The growth temperature determines the growth rate, but also the defects generated during growth; which means that changes in the CL spectrum are observed.
Fig.12 presents the panchromatic CL images of both samples. One observes that faceting is different in sample F4-15-11, however sample F4-12-11, which was also grown at higher temperature presents the typical faceting. A possibility is that in the thick samples the faceting is restored along the growth, in which case the narrow sample represents the faceting in the initial stages of growth. Faceting in sample F4-18-11 is similar to faceting of the samples grown at the standard temperature.

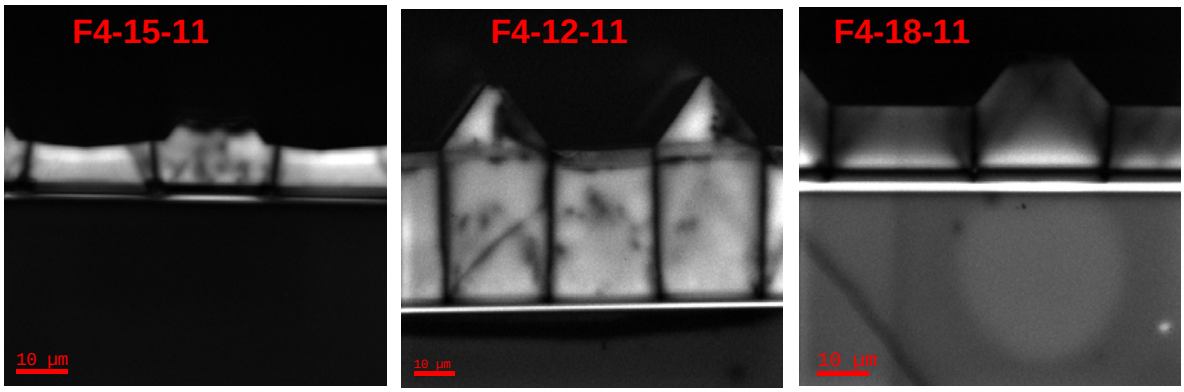

Fig.12. Panchromatic CL images of samples F4-15-11 (high growth temperature, 16µm thick), F4-12-11 (high temperature, 51µm thick), and F4-18-11 (low growth temperature, 15µm thick)

The spectral analysis reveals different incorporation of defects. Typical spectra in the three samples are shown in Fig.13

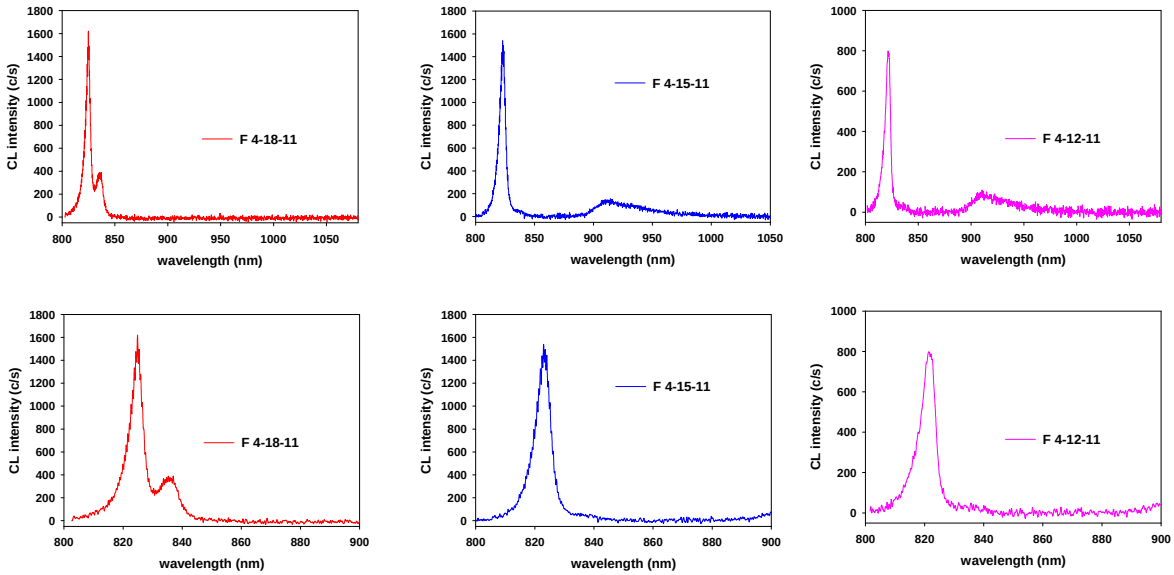

Fig.13. CL spectra recorded in the three samples. The lower spectra correspond to the expanded 800-900 nm spectral window

The samples grown at high temperature present an spectrum similar to the spectrum recorded in samples grown at the standard temperature; with the NBE band and the V_{Ga} complex related bands at 908 nm and 925 nm. The sample grown at low temperature presents a strong eA band in the low energy side of the NBE band, peaking at 1.482 eV which corresponds to e-Si_{As}^{o} transitions. This is interesting, because, it is accompanied by the absence of the band associated with the V_{Ga} complexes, suggesting that under such growth conditions the stoichiometry is Ga rich, which explains the absence of V_{Ga}s, and the As lattice position of the Si atoms at such a low concentration. The

intensity of the Acceptor related band decreases along the growth direction. See the three spectra of Fig. 14, taken close to the interface, and 5 μm, and 10 μm up along the growth axis. One observes a progressive reduction of the acceptor related band, while the Si_{Ga}-V_{Ga} related band peaking at 1.2 eV starts to be observed. This behaviour suggests that the effective [Ga]/[As] flow ratio decreases along the growth run, which could be interpreted by Ga rich parasitic nucleation.

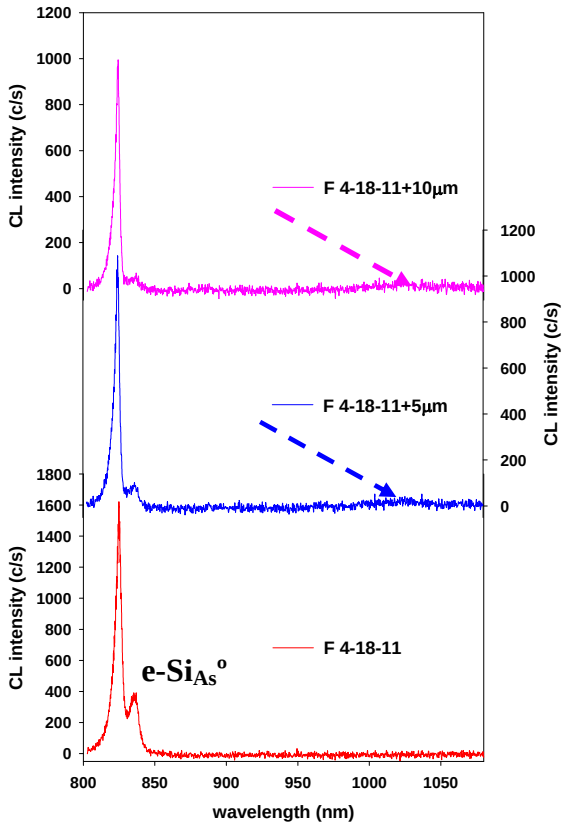

Fig.14. CL spectra recorded at three positions along the growth axis, separated 5μm from each other, showing the evolution of the e-Si_{As}^{o}, and the V_{Ga}-Si_{Ga} (arrows) bands respectively.

Regarding the samples grown at high temperature one can argue that the growth conditions of the two samples, in spite of the thickness, were not similar.
One can observe the local spectra recorded in sample F4-15-11 in Fig. 15. One observes that close to the template, the spectra are very different with a significant incorporation of V_{Ga} related defects (spectra #1, 7, 8); while out of that zone, the bands associated with V_{Ga}s complexes (908 nm and 925 nm) appear with high intensity, which suggests low [Ga]/[As] ratio incorporation.
Sample F412-11 presents characteristics that fit the samples grown in the regular way. Typical spectrum images for the main parameters of this sample are shown in Fig. 16. One observes the NBE emission depletion a the domain wall, the compressive stress deduced from the peak shift, the local enhancement of the 910 nm band along the domain wall, even the local presence of the 950 nm band, usually observed along the domain wall.

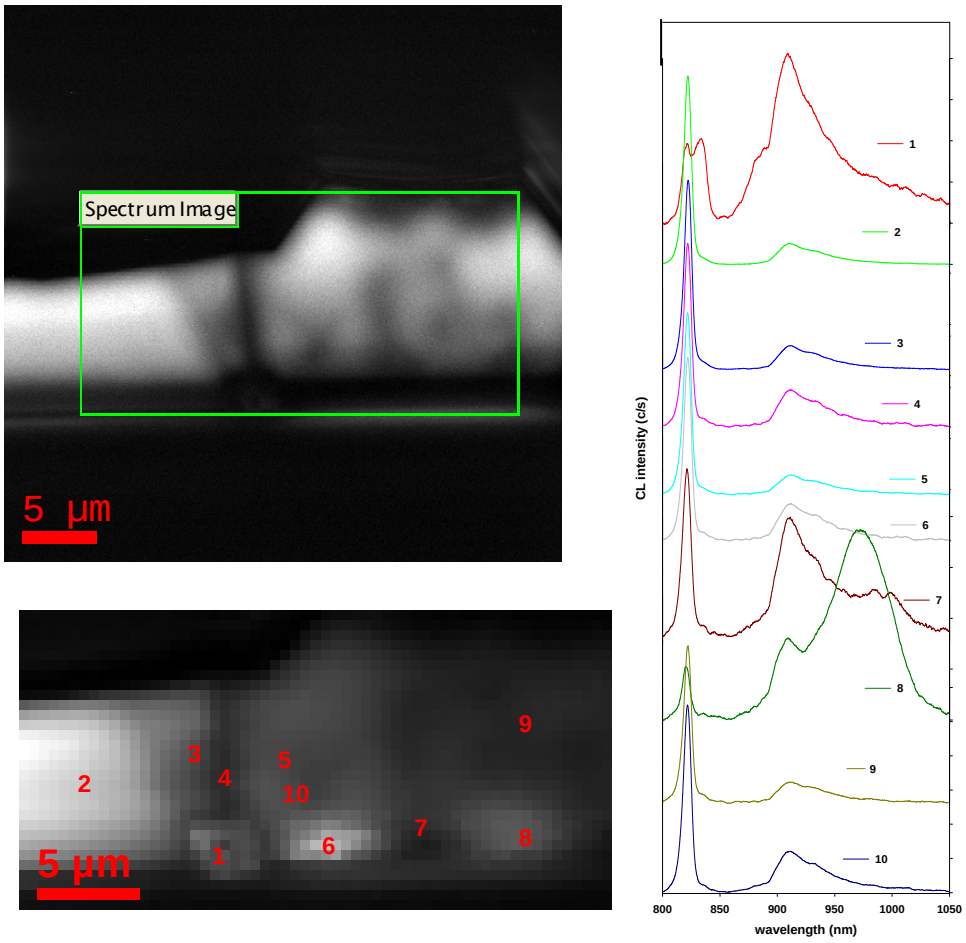

Fig.15. CL images and local spectra recorded at the points marked in the lower CL image (sample F4-15-11)

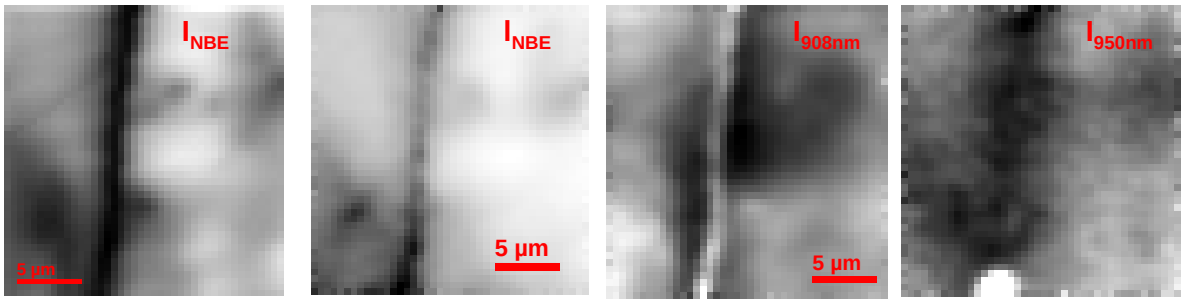

Fig.15. Spectrum images of the domain wall region of sample F4-12-11. Note that the 950 nm band appears in the domain wall in the lower part of the image.

Publications:

1) Growth and characterization of orientation patterned GaAs crystals for non-linear optical frequency conversion; O. Martínez, M. Avella, V. Hortelano, J. Jiménez, M. Snure, C.Lynch, D. Bliss; MRS Symp. Proc.1288, G06 (2011)

2) Spectrally Resolved Cathodo-luminescence imaging study of periodic [001]/[00-1] GaAs structuresfor non linear optical conversion; V. Hortelano, O. Martínez, J. Jiménez, C.Lynch, M .Snure, D. Bliss; Phys.St.Sol.c submitted

3) Cathodoluminescence study of e-irradiated, and plastically deformed ZnO crystals M.Avella, V.Hortelano, O.Martínez, J.Mass, J. Jiménez, B.Wang, P. Drevinsky, and D. Bliss; Phys.St.Sol.c submitted

4) Impurity incorporation in Orientation Patterned GaAs grown by low pressure HVPE; M .Snure, J. V.Hortelano, Jiménez, S. Swider, M. Mann, V. Tassev, C. Lynch, D. Bliss; J. Cryst. Growth submitted

5) Cathodoluminescence study of ammonothermal GaN crystals; V. Hortelano, O.Martínez, J.Jiménez, Buguo Wang, S. Swider, M. Suscavage, D.Bliss; Mater.Sci. Forum submitted

6) Cathodoluminescence characterization of Si-doped orientation patterned GaAs crystals; V. Hortelano, O. Martínez, J. Jiménez, M.Snure, C.Lynch, D. Bliss (to be presented at MRS Fall meeting, oral presentation)